

การประเมินทางเทคนิคของการเกิดภาพแปลกปลอมจากขดลวดในหลอดเลือดของ
สมองของเครื่องถ่ายภาพสนามแม่เหล็กกำลัง 3 เทสลา : การศึกษาในหลอดทดลอง

นายอศุทธ์ กำแพงทิพย์

วิทยานิพนธ์นี้เป็นส่วนหนึ่งของการศึกษาตามหลักสูตรปริญญาวิทยาศาสตรมหาบัณฑิต
สาขาวิชาอายุเวชศาสตร์ ภาควิชารังสีวิทยา
คณะแพทยศาสตร์ จุฬาลงกรณ์มหาวิทยาลัย
ปีการศึกษา 2554
ลิขสิทธิ์ของจุฬาลงกรณ์มหาวิทยาลัย

บทคัดย่อและแฟ้มข้อมูลฉบับเต็มของวิทยานิพนธ์ตั้งแต่ปีการศึกษา 2554 ที่ให้บริการในคลังปัญญาจุฬาฯ (CUIR)
เป็นแฟ้มข้อมูลของนิสิตเจ้าของวิทยานิพนธ์ที่ส่งผ่านทางบัณฑิตวิทยาลัย

The abstract and full text of theses from the academic year 2011 in Chulalongkorn University Intellectual Repository (CUIR)
are the thesis authors' files submitted through the Graduate School.

**TECHNICAL ASSESSMENT OF ARTIFACT PRODUCTION
FROM NEURO ENDOVASCULAR COIL AT 3 TESLA MRI
:AN IN VITRO STUDY**

Mr.Adun Kampaengtip

**A Thesis Submitted in Partial Fulfillment of the Requirements
for the Degree of Master of Science Program in Medical Imaging
Department of Radiology
Faculty of Medicine
Chulalongkorn University
Academic Year 2011
Copyright of Chulalongkorn University**

Thesis Title TECHNICAL ASESMENT OF ARTIFACT
 PRODUCTION FROM NEURO
 ENDOVASCULAR COIL AT 3 TESLA MRI
 AN IN VITRO STUDY


By Mr.Adun Kampaengtip

Field of Study Medical Imaging


Thesis Advisor Associate Professor Anchali Krisanachinda, Ph.D.


Thesis Co-advisor Associate Professor Sirintara Singhara Na Ayudya,
 M.D.


Accepted by the Faculty of Medicine, Chulalongkorn University in
Partial Fulfillment of the Requirements for the Master's Degree

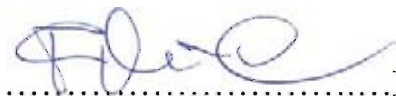

.....Dean of the Faculty of Medicine
(Associate Professor Sophon Napathorn, M.D.)

THESIS COMMITTEE


.....Chairman
(Assisstant Professor Jarturon Tantivatana, M.D.)


.....Thesis Advisor
(Associate Professor Anchali Krisanachinda, Ph.D.)


.....Thesis Co-advisor
(Associate Professor Sirintara Singhara Na Ayudya, M.D.)


.....External Examiner
(Professor Franco Milano, Ph.D.)

อดุลย์ กำแพงทิพย์: การประเมินทางเทคนิคของการเกิดภาพแปลกปลอมจากการใส่ขดลวดในหลอดเลือดของสมองของเครื่องถ่ายภาพสนามแม่เหล็กกำลัง 3 เทสลา: การศึกษาในหุ่นจำลอง. (Technical Assessment of Artifact Production from Neuro Endovascular Coil at 3 Tesla MRI: An In Vitro Study) อ. ที่ปรึกษาวิทยานิพนธ์หลัก: รศ. ดร. อัญชติ กฤษณจินดา, อ. ที่ปรึกษาวิทยานิพนธ์ร่วม: รศ. พญ. ศิรินธรา สิงหรา ณ อยุธยา, 75 หน้า.

ในช่วงหลายปีที่ผ่านมาเครื่องสนามแม่เหล็กกำลัง 3 เทสลา (MRI) มีการใช้งานมากขึ้นและแพร่หลายมากขึ้นเนื่องจากอัตราส่วนของสัญญาณสูง (SNR). หนึ่งในภาพแปลกปลอมในภาพของเครื่องแม่เหล็กกำลัง 3 เทสลาเกิดจากขดลวดทางรังสีร่วมรักษาเพิ่มขึ้น โดยที่เกิดจากความไม่สม่ำเสมอของสนามแม่เหล็กในบริเวณที่มีขดลวด. การสูญเสียสัญญาณในบริเวณดังกล่าว เกิดในภาพสนามแม่เหล็กกำลัง 3 เทสลา ประกอบด้วยพื้นที่ของสัญญาณที่หายไปกับบริเวณโดยรอบของความเข้มของสัญญาณที่เพิ่มขึ้นที่ปรากฏจะทำให้ใหญ่กว่าขนาดที่แท้จริงของอุปกรณ์ที่ก่อให้เกิดภาพแปลกปลอม. ความถี่ของสัญญาณวิทยุถูกดูดกลืนโดยโลหะถูกทดสอบที่ความเข้มสนามแม่เหล็ก 3 เทสลา. การวิเคราะห์ภาพแปลกปลอมที่มีความสัมพันธ์ภาพสำหรับขดลวดที่เพิ่มขึ้นโดยเฉลี่ย วัตถุประสงค์ของการศึกษาคือการเปรียบเทียบขนาดของภาพแปลกปลอมที่เกี่ยวกับภาพเปรียบเทียบกับขนาดแท้จริงของขดลวดที่ใช้เพิ่มขึ้น โดยเฉลี่ยของเครื่องแม่เหล็กกำลัง 3 เทสลา เป็นการศึกษาในหลอดทดลอง ขดลวดขนาดต่างๆ ทำจากขดลวด พลาตินัม, หลอดเลือดโป่งพองจำลองสร้างโดยใช้ท่อซิลิโคน ระบบของเครื่องแม่เหล็กกำลัง 3 เทสลา ยี่ห้อฟิลิปส์ รุ่น Achieva, วิธีลำดับพัลส์: Spin echo, Fast spin echo, Inversion recovery, และ Fast gradient echo. ทำการศึกษาพารามิเตอร์ที่มีผลกับการเกิดภาพแปลกปลอมเพิ่มเติม ได้แก่ Echo time (TE) และ Turbo factor

ในการวิจัยในครั้งนี้เป็นการศึกษาการนอกร่างกายมนุษย์, เราได้กำหนดไว้บางส่วนของคุณลักษณะสำคัญที่เกี่ยวข้องกับภาพของเครื่องสนามแม่เหล็กกำลัง 3 เทสลา ของขดลวด การสร้างภาพที่ดีของเนื้อเยื่อสมองรอบๆขดลวดและหลอดเลือดโป่งพอง สามารถทำได้ดีที่สุดโดยวิธีลำดับพัลส์ Spin echo ซึ่งเป็นไปอย่างมีนัยสำคัญ ($P \leq 0.05$), วิธีลำดับพัลส์ Fast spin echo, Inversion recovery และ Fast gradient echo ตามลำดับ. วิธีลำดับพัลส์ Fast gradient echo เป็นวิธีที่ทำให้เกิดภาพแปลกปลอมได้มากที่สุด. ข้อเสนอแนะจากการศึกษานี้คือ; 1) ภาพแปลกปลอมเกิดน้อยที่สุดที่ วิธีลำดับพัลส์ Spin echo วิธีลำดับพัลส์ Fast spin echo ควรเลือก Turbo factor สั้น; 2) การลด TE ที่เป็นปัจจัยหลักในการปรับปรุงการเกิดภาพแปลกปลอม ในภาพเป็นไปอย่างมีนัยสำคัญ ($P \leq 0.05$), หลอดเลือดโป่งพอง ที่มีความหนาแน่นสูงกว่าของขดลวดทำให้ผลผลิตภาพแปลกปลอมมากขึ้นภายใต้เงื่อนไขทั้งหมด สุดท้ายการเกิดภาพแปลกปลอมจากขดลวดจะเกิดในทิศทางการเข้ารหัสความถี่ (frequency encoding).

ภาควิชา รังสีวิทยา ลายมือชื่อนิสิต *อดุลย์ กำแพงทิพย์*
 สาขาวิชา ฉายาเวชศาสตร์ ลายมือชื่อ อ. ที่ปรึกษาวิทยานิพนธ์หลัก *ดร. อัญชติ*
 ปีการศึกษา 2554 ลายมือชื่อ อ. ที่ปรึกษาวิทยานิพนธ์ร่วม *ดร. พญ. ศิรินธรา*

5374670330 : MAJOR MEDICAL IMAGING

KEYWORDS : MRI 3 TESLA / SUSCEPTIBILITY ARTIFACT/ COIL PACKS

ADUN KAMPAENGTIP: TECHNICAL ASSESSMENT OF ARTIFACT
 PROCUTION FROM NEURO ENDOVASCULAR COIL AT 3 TESLA MRI
 : AN IN VITRO STUDY. ADVISOR: ANCHALI KRISANACHINDA, Ph.D,
 CO-ADVISOR SIRINTARA SINGHARA NA AYUDYA, M.D, 75 pp.

Magnetic resonance imaging (MRI) is an essential part in diagnostic radiology and post-treatment valuation. MRI 3 Tesla is becoming more and more widespread due to high signal to noise ratio (SNR). The artifact in magnetic resonance imaging results from endovascular coils. Susceptibility artifacts and geometric distortions caused by magnetic field inhomogeneity- related signal loss is used to refer to an artifact in magnetic resonance images. It consists of a region of signal void with a surrounding area of an increased signal intensity that appears to be considerably larger than the actual size of the device causing the artifact. RF metal interaction effects were investigated systematically at $B_0 = 3$ Tesla, analyzing correlated image artifacts for endovascular coils. The objective of the study is to compare the size of the artifact on the MR image to the actual size of endovascular coils using a 3 Tesla magnetic resonance imaging system, in vitro study. Endovascular coils were made from detachable platinum coils and aneurysm models were constructed by using catheters. A drop of gadolinium in normal saline solution was injected into each catheter. MRI 3 Tesla Philips Model Achieva. Pulse sequence selections were: Spin echo (conventional), fast spin echo, Inversion Recovery, Fast Gradient echo while additional parameters were Echo time and Turbo Factor.

Improved visualization of peri-aneurysmal soft tissues is best accomplished by Spin echo and Fast spin echo sequences are even better suited to reduce metal artifact. Furthermore, shorter turbo factor and shorter effective TE in the latter sequences are beneficial for the same reason as sequences having shorter TE. Sequences with a shorter TE are preferred because there is less time for dephasing and frequency shifting. Imaging at gradient echo series increases susceptibility artifacts. In this in vitro study, we have defined some of the major characteristics related to MRI imaging of coil packs. conclusions from this study are; 1) Pulse sequence Spin echo is best reduce susceptibility artifact; 2) Reducing the TE is the main factor in improving peri-aneurysmal visualization on MRI images; 3) The use of small field of view, high resolution matrix and thin slice can help reduce susceptibility artifacts. Artifacts are also produced in the frequency encoding

Department : Radiology Student's Signature *Adun K.*

Field of Study : ... Medical Imaging ... Advisor's Signature *Anchali K.*

Academic Year : 2011 Co-advisor's Signature *Sirintara Singhara Na Ayudya*

ACKNOWLEDGEMENTS

I would like to express gratitude and deepest appreciation to Associate Professor Anchali krisanachinda, Ph.D., Division of Nuclear Medicine, Department of Radiology, Faculty of Medicine, Chulalongkorn University, My advisor, for her guidance, helpful suggestion, supervision, constructive comments and polishing of the thesis writing to improve the readability and English expression.

I would like to extremely greatly Associate Professor Sirintara singhara Na Ayudya, M.D., Division of Diagnostic Radiology, Department of Radiology, Faculty of Medicine, Ramathibodi Hospital, Mahidol University, for advice and comments in the research

I would like to extremely greatly Associate Professor Sivalee Suriyapee, M.Sc., Division of Radiation Oncology, Department of Radiology, Faculty of Medicine, Chulalongkorn University, My teacher, for her invaluable advices, constructive comments.

I would like to extremely greatly Mr. Taweep Sanghangthum, M.Sc., Mr. Sornjarod Oonsiri, M.Sc., Ms. Puntawa Insang, M.Sc., the medical physic staffs at Division of Radiation Oncology, Department of Radiology, Faculty of Medicine, Chulalongkorn University, for their invaluable advices, constructive comments.

I would like to deeply thank Professor franco Milano, Ph.D. from University of Florence Italy, who external examiner of this thesis defense for this helpful concentrate of recommendation, constructive comments and teaching of knowledge in Medical Imaging.

I would like to thank Mrs. Weeranuch Kitsukjit for her provide suggestion for the improvement. I am thankful for all teachers, lectures and staff in the Master of Science Program in Medical Imaging, Faculty of Medicine, Chulalongkorn University.

Finally, I am extremely gremely grateful for all teachers. Lecturers and straffs at Master of science Program in Medical Imaging, Faculty of Medicine, Chulalongkorn University for their help, and unlimited teaching of knowledge during the course in Medical Imaging. My grateful is forwarded to the Graduate Studies for supply the knowledge as tutor, especially, Mr. Kitiwat Khamwan for him contribution in part data analysis and every suggestion and Advanced diagnostic Imaging and Image-guided Minimal Invasive Center for their kind supports.

CONTENTS

	Page
ABSTRACT (THAI).....	iv
ABSTRACT (ENGLIST).....	v
ACKNOWLEDGEMENT.....	vi
CONTENTS.....	vii
LIST OF TABLES.....	xii
LIST OF FIGURES.....	xiii
LIST OF ABBREVIATIONS.....	xiv
CHAPTER I INTRODUCTION	
1.1 Background and rationale.....	1
1.2 Research Objective.....	2
CHAPTER II REVIEW OF RELATED LITERATURES	
2.1 Theory.....	3
2.1.1 The introduction of MRI.....	3
2.1.2 Resonance and Relaxation.....	3
2.1.3 Spatial Encoding.....	8
2.1.4 Imaging Contrast.....	11
2.1.5 MR equipment.....	13
2.1.6 MRI Artifacts.....	15
2.1.7 MRI 3 Tesla and Susceptibility artifact.....	18
2.1.8 Introduction of Neuro endovascular Intervention.....	20
2.2 Review of Related Literature.....	21
CHAPTER III RESEARCH METHODOLOGY	
3.1 Research Design.....	24
3.2 Research Design Model.....	24
3.3 Conceptual Framework.....	24
3.4 Research Questions.....	25
3.4.1 Primary Question.....	25
3.5 Materials.....	25
3.5.1 MRI 3.0 Tesla, Philips: Achieva.....	25
3.5.2 8-Channel SENSE Head coil.....	25

	Page
3.5.3 Endo neurovascular coils.....	26
3.5.4 ACR MRI phantom.....	26
3.5.5 Vascular phantom.....	27
3.5.6 Advantage Workstation.....	27
3.5.7 SPSS program.....	28
3.6 Methods.....	28
3.6.1 QC for MRI scanner.....	28
3.6.2 The characteristics of Susceptibility artifact of Endovascular Coils.....	28
3.6.2.1 MRI Scanning techniques.....	28
3.6.3 Quantitative assessment.....	29
3.6.4 Assessment of the Neuro endovascular coils packs and Susceptibility artifact and measurement of image artifact for MRI 3.0 Tesla....	29
3.7 Data analysis.....	30
3.7.1 Image Evaluation.....	30
3.7.2 Diameter and Volume measurement.....	30
3.8 Sample size determination.....	30
3.9 Statistical analysis.....	30
3.10 Outcome measurement.....	30
3.11 Expected benefits.....	30
3.12 Ethical consideration.....	31
CHAPTER IV RESULTS	
4.1 Quality control of MRI scanners.....	32
4.2 Diameter Measurement Data.....	32
4.2.1 Evaluation of the artifact diameter.....	32
4.3 Volume Measurement Data.....	43
4.3.1 Evaluation of the artifact volume.....	43
4.4 Quantitative assessment.....	47
CHAPTER V DISCUSSION AND CONCLUSION	
5.1 Discussion.....	50
5.1.1 Assessment of susceptibility artifact in Pulse sequence....	50

	Page
5.1.2 Assessment of susceptibility artifact in Turbo factor	52
5.1.3 Assessment of susceptibility artifact in Voxel size.....	52
5.1.4 Assessment of susceptibility artifact in Echo time (TE)...	54
5.1.5 Frequency Encoding Direction.....	55
5.1.6 Overestimation Factor.....	56
5.1.7 Clinical Relevance.....	56
5.1.8 Sequence development.....	57
5.2 Study Limitations.....	57
5.3 Conclusions.....	57
REFERENCES	59
APPENDICES	61
Appendix A.....	62
Appendix B.....	64
VITAE	75

LIST OF TABLES

Table	Page
3.1 The MRI scanning technique at MRI 3.0 T.....	29
4.1 Report of MRI systems 3.0 T performance test.....	32
4.2 Percent error in pulse sequence of signal loss due to coil-induced in susceptibility artifact when compared to actual size of coils pack dimension of 2.0x2.0x5.0 mm.....	33
4.3 Percent error in pulse sequence of signal loss due to coil-induced susceptibility artifact actual size of coil pack dimension 5.6x5.6x9.8 mm.....	33
4.4 Percent error in pulse sequence of signal loss due to coil-induced susceptibility artifact actual size of coil pack dimension 7.6x6.5x9.0 mm.....	34
4.5 Percent error of artifact diameter versus echo time (ms) for fast spin echo, of signal loss due to coil-induced susceptibility artifact.....	35
4.6 Percent error of artifact diameter versus echo time (ms) for fast spin echo, of signal loss due to coil-induced susceptibility artifact.....	35
4.7 Percent error of artifact diameter versus echo time (ms) for fast spin echo, of signal loss due to coil-induced susceptibility artifact.....	36
4.8 Percent error of artifact diameter versus echo time (ms) for fast gradient echo, of signal loss due to coil-induced susceptibility artifact.	37
4.9 Percent error of artifact diameter versus echo time (ms) for fast gradient echo, of signal loss due to coil-induced susceptibility artifact.	38
4.10 Percent error of artifact diameter versus echo time (ms) for fast gradient echo, of signal loss due to coil-induced susceptibility artifact.	39
4.11 Percent error of artifact diameter versus turbo factor for fast spin echo, of signal loss due to coil-induced susceptibility artifact.....	40
4.12 factor for fast Percent error of artifact diameter versus turbo spin echo, of signal loss due to coil-induced susceptibility artifact.....	41
4.13 Percent error of artifact diameter versus turbo factor for fast spin echo, of signal loss due to coil-induced susceptibility artifact.....	42
4.14 Volume overestimation factor (mm ³); in pulse sequence due to coil-induced susceptibility artifact actual size of coil volume (26 mm ³).....	46
4.15 Volume overestimation factor (mm ³); in pulse sequence due to coil-induced susceptibility artifact actual size of coil volume (160 mm ³)....	46
4.16 Volume overestimation factor (mm ³); in pulse sequence due to coil-induced susceptibility artifact as actual size of coil volume (229 mm ³).	47
4.17 The data for quantitative assessment of signal intensity loss as three planes diameter. The actual size of coil volume 26 mm ³	47

Table	Page
4.18 The data for quantitative assessment of signal intensity loss as three planes diameter. The actual size of coil volume 160 mm ³	48
4.19 The data for quantitative assessment of signal intensity loss as three planes diameter. The actual size of coil volume 229mm ³	48
4.20 The data for quantitative assessment of signal intensity loss as three volume size of coil packs. The actual size of coil volume 229 mm ³	49
5.1 Overestimation factors.....	56

LIST OF FIGURES

Figure	Page
2.1 Two possible orientations for the proton in an external magnetic field.....	4
2.2 Precession of the magnetic moment.....	5
2.3 A collection of spins at any given instant in an external magnetic field, B_0	6
2.4 The effect of RF radiation on the net magnetization.....	7
2.5 After a 90 degrees RF pulse.....	8
2.6 Spin echo diagram.....	8
2.7 The addition property of the Fourier transforms.....	11
2.8 Basic magnet component of an MR system.....	13
2.9 Maxwell pair configuration for a longitudinal (Z) gradient field.....	14
2.10 Golay coils configuration for transverse (x and y) gradient fields.....	14
2.11 Phase sampling/phase wrap artifact.....	16
2.12 Susceptibility artifact.....	16
2.13 Zipper artifacts.....	17
2.14 Truncation artifacts.....	18
2.15 Transverse T1-weighted gradient-echo MR images.....	19
2.16 Coil procedures for cerebral Aneurysm.....	20
3.1 MRI 3.0 Tesla.....	25
3.2 8-Channel SENSE Head coil.....	25
3.3 Endo neurovascular coil.....	26
3.4 ACR MRI phantom.....	26
3.5 Silicone tube.....	27
3.6 Advantage workstation program.....	27
4.1 The percent error of artifact diameter for fast spin echo versus echo time (ms) in three orthogonal planes from 2.0x2.0x5.0 mm.....	35
4.2 The percent error of artifact diameter versus echo time for fast spin echo in three orthogonal planes of 5.6x5.6x9.8 mm.....	36
4.3 The percent error of artifact diameter versus echo time for fast spin echo in three orthogonal planes of 6.5x6.5x9.0 mm.....	37
4.4 The percent error of artifact diameter versus echo time for fast gradient echo in three orthogonal planes of 2.0x2.0x5.0 mm.....	38
4.5 The percent error of artifact diameter versus echo time for fast gradient echo in three orthogonal planes of 5.6x5.6x9.8 mm.....	39
4.6 The percent error of artifact diameter versus echo time for fast gradient echo in three orthogonal planes of 6.5x6.5x9.0 mm.....	40
Figure	Page
4.7 The percent error of artifact diameter versus turbo factor for fast spin echo in three orthogonal planes of 2.0x2.0x5.0 mm.....	41

4.8	The percent error of artifact diameter versus turbo factor for fast spin echo in three orthogonal planes of 5.6x5.6x9.8 mm.....	42
4.9	The percent error of artifact diameter versus turbo factor for fast spin echo in three orthogonal planes of 6.5x6.5x9.0 mm.....	43
4.10	The signal loss volumes (mm^3) versus pulse sequence at different, matrix size and slice thickness of volume of coil pack 26 mm^3	44
4.11	The signal loss volumes (mm^3) versus pulse sequence, matrix size and slice thickness of volume of coil pack 160 mm^3	44
4.12	The signal loss volumes (mm^3) versus pulse sequence at different, matrix size and slice thickness of volume of coil pack 229 mm^3	45
5.1	The image of susceptibility artifact from Aluminum.....	50
5.2	Image of neuro endovascular coil from Spin echo.....	51
5.3	The susceptibility artifacts of Spin echo.....	52
5.4	Susceptibility artifacts from Turbo factor.....	52
5.5	Susceptibility artifacts between Slice thickness.....	53
5.6	Susceptibility artifacts between matrix sizes.....	53
5.7	Susceptibility artifacts between Fast spin echo sequence Echo time...	54
5.8	Susceptibility artifacts between fast gradient echo sequence Echo time.....	54
5.9	The susceptibility artifacts in three orthogonal planes.....	55

LIST OF ABBREVIATION

ABBREVIATION	TERMS
AAPM	American Association of Physicists in Medicine
ACR	American College of Radiology
ANOVA	Analysis of Variant
B_0	Magnetic field strength
B_1	Radio frequency field strength
C°	Degree celcius
CM	Classical mechanics
CT	Computed tomography
DWI	Diffusion weight image
FGRE	Fast gradient echo
FID	Free induction decay
fMRI	Function magnetic resonance imaging
FOV	Field of view
FSE	Fast spin echo
IR	Inversion recovery
MARS	Metal artifact reduction sequence
MRA	Magnetic resonance angiogram
MRI	Magnetic resonance imaging
MRS	Magnetic resonance spectroscopy
NSA	Number of average
RF	Radiofrequency
SE	Spin echo
TE	Echo time
TOF	Time of flight
TR	Repetition time
μT	Micro Tesla
VAT	View angle tilting

CHAPTER I

INTRODUCTION

1.1 Background and Rationale

Magnetic resonance imaging (MRI) systems at field strength, B_0 , of 3 Tesla become more and more frequent use in recent years. With the increasing number of radiological sites, 3-Tesla MRI starts to play the same role for clinical imaging that was occupied by 1.5-Tesla systems for the last 10 years¹⁻¹⁰. The main motivation for the transition from 1.5-Tesla to 3-Tesla MRI systems is the improved signal to-noise ratio (SNR), which is approximately proportional to the field strength¹¹, B_0 ; thus, under the ideal conditions and with optimized acquisition techniques a doubled SNR can be expected at 3 Tesla in comparison to 1.5 Tesla. The growing availability of 3-Tesla MRI systems is, for instance, demonstrated by the number of publications on 3-Tesla MRI listed in the Medline database, which increased from around 30 in the year 2000 to more than 400 in 2006. In the 1990s, 3-Tesla MRI was available predominantly in a small number of specialized neuroradiological or neuropsychiatric research sites.

Typical applications including functional MRI or spectroscopy studies of the brain were performed with optimized protocols under the attendance of specialized engineers or physicists. Today, the availability of 3-Tesla MRI systems has substantially broadened for imaging of all anatomical areas including musculoskeletal, abdominal, cardiac, angiographic and whole-body imaging. This development leads to an increasing diversity of applied pulse sequences and protocols, which are not always fully optimized for 3-Tesla MRI. Consequently, the radiologist or technician working with such 3-Tesla protocols will be confronted with image artifacts related to 3-Tesla MRI.

Endovascular therapy is a minimally invasive procedure that accesses the treatment area from within the blood vessel. In the case of aneurysm, this treatment is referred to coil embolization, or "coiling". In contrast to surgery, endovascular coiling does not require open surgery. Instead, physicians use fluoroscopic imaging to visualize the patient's vascular system and treat the disease from inside the blood vessel.

Endovascular treatment of brain aneurysm involves the insertion of a catheter, small plastic tube, into the femoral artery in the patient's leg and navigating it through the vascular system, into the head and aneurysm. Tiny platinum coils are threaded through the catheter and deployed into the aneurysm, blocking blood flow into the aneurysm and preventing rupture. The platinum coil can be visible via X-ray fluoroscopy and be flexible enough to conform to the aneurysm shape.

Endovascular coil embolization of the brain aneurysm is safe and effective; aneurysm recurrent remains a limitation requiring surveillance imaging. Recently MR angiography has become a viable option for non-invasive follow-up. Often, a base line MRA within one week of coiling is acquired for comparison. The coil mass

products magnetic susceptibility artifact may obscure the evaluation of the host vasculature and the aneurysm.

Magnetic susceptibility artifact refers to the internal magnetization of a substance when it is placed in a magnetic field. Since MRI scanner needs a homogenous magnetic field to create accurate images, any distortion of the magnetic field will lead to an artifact [9].

Although previous research in MR artifact has been done in vitro, the dynamic characteristics of a functional vascular system cannot be stimulated. The aim of this study is to evaluate the MR susceptibility artifact from various platinum coil sizes overtime using different MRI technique.

1.2 Research Objective

1.2.1 To compare the actual size of the endovascular coil and size of the susceptibility artifact.

1.2.2 To determine the factors affecting the artifact from endovascular coil (pulse sequence, matrix size, slice thickness, turbo factor and echo time).

CHAPTER II

REVIEW OF RELATED LITERATURES

2.1 Theory

2.1.1 The introduction of MRI [1]

The Magnetic Resonance Imaging (MRI) was discovered in the 1950s and for many years its major application was in the field of spectroscopy; discerning chemical species from the inherent shift in resonant frequency exhibited by nuclei which depends on their chemical environment. Until the 1970s when Lauterbur introduced the concept of magnetic field gradients, an image based on magnetic resonance could be produced. By the 1980s whole body magnets were being produced in England permitting the first in vivo images of human anatomy. Today the technique, known as MR imaging, is widespread and an estimated 20 million scans are performed worldwide each year. It provides images with excellent soft-tissue contrast which can be acquired in any imaging plane, and unlike CT it does not involve the use of ionizing radiation. It is the imaging modality of choice in brain spinal cord and musculoskeletal for routinely use in many other clinical settings.

Magnetic resonance imaging (MRI) has provided high temporal, spatial, and contrast resolution methods to assess structure. However, the need to assess beyond the purely anatomic aspects, such as biochemistry and tissue physiology, required the development of functional techniques such as functional magnetic resonance imaging (fMRI), perfusion weighted imaging (PWI), and diffusion weighted imaging (DWI), and magnetic resonance spectroscopy (MRS).

In selecting pulse sequences and measurement parameters for a specific application, MRI allows the user tremendous flexibility to produce variation in contrast between normal and diseased tissue. This flexibility is available when imaging both stationary tissues as well as flowing blood. For example: technique bright-blood and dark-blood. A typical patient examination acquires sets of images with multiple types of contrast (proton density, T1, T2) and multiple slice orientations (transverse, sagittal, coronal, oblique), providing the clinician with more complete information on the nature of the tissue under observation and increasing the likelihood of lesion detection. It is important that the MR examinations be tailored to the organ or organs under investigation, the type of disease process, and the individual patient. The MR physician may choose to provide detailed measurement parameters for each examination, or have a predetermined regimen of scans performed by a technologist. Establishing fixed measurement protocols to ensure reliable, reproducible imaging examinations are performed.

2.1.2 Resonance and Relaxation [2]

Spinning nuclei: Atom consists of electrons orbiting a central nucleus of neutrons and protons known as fundamental particles. MRI is derived from NMR, nuclear magnetic resonance. In particular the nucleus of the hydrogen atom, because its abundant in the human body is a single positively charged proton. Fundamental

particles spin on their own axes, and the hydrogen nucleus is thus a continuously rotating positive charge. From basic electromagnetism, a moving charge has an associated magnetic field and the proton generates its own tiny field known as its magnetic moment.

If the proton is placed in a strong external magnetic field, it experiences a turning force, known as a torque. This is similar to a compass needle which experiences a force in the Earth's magnetic field and turns so that it is aligned with the direction of the field, but it is constrained by the laws of quantum mechanics (QM). Quantum mechanics is a branch of physics which explains the rather odd behavior of very small particles such as protons and electrons, which sometimes act like particles and sometimes like waves. Classical mechanics (CM) on the other hand works for normal-sized (macroscopic) bodies, and for large numbers of small particles where their quantum mechanical behavior is averaged out. Although we have to do a bit of QM to understand why the protons don't simply align with the field, we will find that CM is quite capable of explaining almost everything else.

Since it can't align exactly with the external field, the proton continues to experience a torque which makes it precess around the direction of the wobbling of a spinning top (gyroscope) tilted slightly off axis so that it experiences a torque due to gravity.

The precessional frequency of the protons is found to be proportional to the external magnetic field, given by the Larmor equation

$$\omega_0 = \gamma B_0$$

Where γ is a constant called the gyromagnetic ratio, equal to $2.7 \times 10^8 \text{ rad s}^{-1} \text{ T}^{-1}$. The ω to denote angular frequencies which are vectors, but we are more used to scalar frequencies denoted f ; in these terms the gyromagnetic ratio is 42.57 MHz T^{-1} . The proton in a magnetic field all precess at the same Larmor frequency, not any old frequency. This is known as a resonance condition.

Quantum mechanics explanation: The proton's spin is to be quantized in the presence of an external field, and the torque it experiences makes it precess in one of only two orientations, known in QM as *states*. One state is almost aligned with the other state almost opposite to the external field, known as spin-down or anti-parallel (figure 2.1). Since the magnetic moment is at an angle to the external field, the tip of its vector traces out a circle around the direction of the field (figure 2.2) whichever orientation it is in.

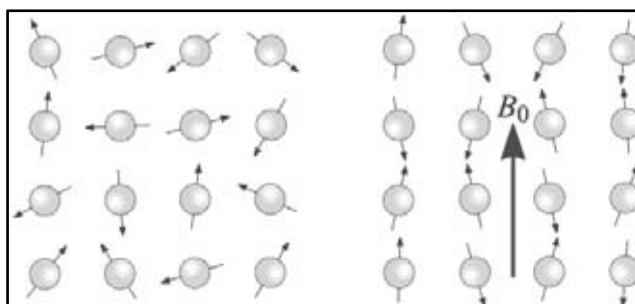


Figure 2.1 Two possible orientations for the proton in an external magnetic field.

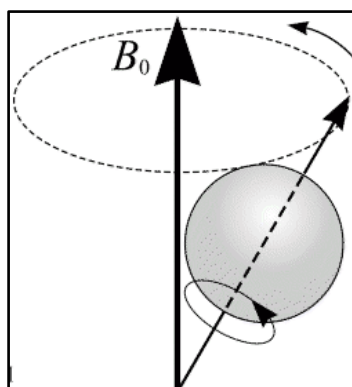


Figure 2.2 Precession of the magnetic moment [3].

The proton which orientation to precess it just depends on how much energy it has since the anti-parallel direction requires slightly more energy than the parallel direction. Both states are stable, so protons are quite happy to stay in either position. However, protons can swap between the two states simply by gaining or losing a certain amount of energy in the form of a photon. It turns out that the energy difference between the two states is directly proportional to the strength of the external magnetic field, and from QM we can calculate exactly what the energy difference is, and thus the frequency of electromagnetic radiation required. The frequency is the Larmor frequency from classical mechanics,

$$\omega_0 = \gamma B_0$$

The classical and quantum mechanical pictures, showing that the precessional frequency of the proton in a magnetic field is the same as the frequency of radiation required to cause transitions between the two states.

In the human body there are many millions of protons; about 75% of water. Although an individual proton obeys QM, it expects to measure their average behavior with CM. There is a statistical distribution of protons between the two state and we find that the lower-energy state is slightly favored, so that there are more protons spinning parallel than anti-parallel. The ratio of the number of spin-up to spin-down protons is given by the following equation which is known as the Boltzmann equation.

$$N_{\text{up}} / N_{\text{down}} = \exp\left(\frac{\gamma \hbar B_0}{kT}\right)$$

At body temperature (37 °C) and 1.5 T scanners, this works out at about 1.000004, which means that for every million protons in the spin-down direction there are a million-and-four protons in the spin-up direction.

In equilibrium the protons are all out of phase with each other, so the tips of the magnetic moment vectors are evenly spread out around the circles. Since there are so many protons, we can make each vector represent the average magnetic moment of a large group of protons all precessing at exactly the same frequency, rather than an individual proton's magnetic moment. This is sometimes called an „isochemat' of protons or term „spin'. This may seem like an unnecessary complication but it means

that we can drop QM and just use CM from now. The vector sum of all these spins is called the net magnetization M_0 which is aligned exactly with the main field B_0 (conventionally shown as the z direction). M_0 is a measurable magnetization which can be calculated to be of the order of microtesla (μT) [2].

Radiofrequency field and MR signal: For a collection of ^1H nuclei, let the number of spins adopting the parallel and anti-parallel states be P_1 and P_2 respectively, with corresponding energy levels E_1 and E_2 . E_2 is greater than E_1 causing P_1 to be greater than P_2 . An obvious question is why do spins adopt the higher energy anti-parallel state? The answer is that spins of P_2 may move to P_1 if the exact amount of energy, $\Delta E = E_2 - E_1$ is supplied to the system. If the temperature of the system were absolute zero, all spins would adopt the parallel orientation. Thermal energy will cause P_2 to be populated. At room temperature in a 1.5 Tesla magnetic field, there will typically be a population ratio $P_2:P_1$ equal to 100,000:100,006.

At any given instant, the magnetic moments of a collection of ^1H nuclei can be represented as vectors, as shown in Figure 2.3. Every vector can be described by its components perpendicular to and parallel to B_0 . For a large number of spins distributed on the surface of the cone, individual components perpendicular to B_0 cancel, leaving only components in the direction parallel to B_0 . As most spins adopt the parallel rather than the anti-parallel state, the net magnetization M is in the direction of the B_0 field.

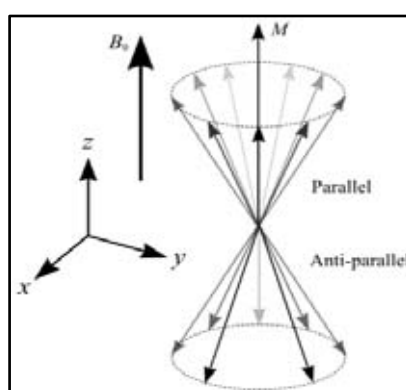


Figure 2.3 A collection of spins at any given instant in an external magnetic field, B_0 . A small net magnetization, M , is detectable in the direction of B_0 [3].

Suppose the direction of B_0 is aligned with the z -axis of Euclidean 3-space, the plane perpendicular to B_0 contains the x and y -axes. In order to detect a signal from ^1H nuclei, radio frequency (RF) energy must be applied. RF energy at the Larmor frequency causes nuclear spins to swap between parallel and anti-parallel states. This has an oscillatory effect on the component of M parallel to the z -axis. RF energy, like all electromagnetic radiation, has electric and magnetic field components. Suppose the magnetic field component is represented by B_1 and lies in the x - y plane, the x - y components of M will be made coherent by the B_1 field giving a net x - y component to M and hence effectively causes M to tilt from the z direction into the x - y plane. This phenomenon is described further in Figure 2.4.

The angle through which M has rotated away from the z -axis is known as the flip angle. The strength and duration of B_1 determine the amount of energy available to achieve spin transitions between parallel and anti-parallel states. Thus, the flip angle is proportional to the strength and duration of B_1 . After pulses of 90 degrees and 270 degrees, M has no z component and the population ratio $P_2:P_1$ is exactly one. A pulse of 180 degrees rotates M into a position directly opposite to B_0 , with greater numbers of spins adopting anti-parallel (rather than parallel) states. If the B_1 field is applied indefinitely, M tilts away from the z -axis, through the x - y plane towards the negative z direction, and finally back towards the x - y plane and z -axis (where the process begins again).

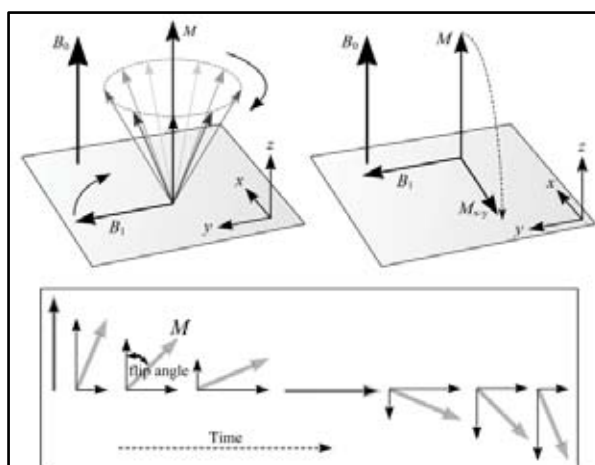


Figure 2.4 (Top) The effect of RF radiation on the net magnetization M is to produce a second magnetic field M_{x-y} . M is tilted from its original longitudinal z -axis orientation, along the direction of the external magnetic field B_0 , into the transverse x - y plane. (Bottom) an illustration of flip angle which is the angle through which M has rotated away from the z -axis [3].

The situation after an RF pulse is applied that causes the net magnetization vector M to flip by 90 degrees (Figure 2.5a). M lies in the x - y plane and begins to precess about the B_0 axis. M will induce an electromotive force in a receiver coil according to Faraday's law of magnetic induction. This is the principle of NMR signal detection. It is from this receiver RF signals that an MR image can be constructed. Figure 2.5(b) shows a graph of the voltage or signal induced in a receiver coil versus time. Such a graph, or waveform, is termed free induction decay (FID). The magnitude of the generated signal depends on the number of nuclei contributing to produce the transverse magnetization and on the relaxation times.

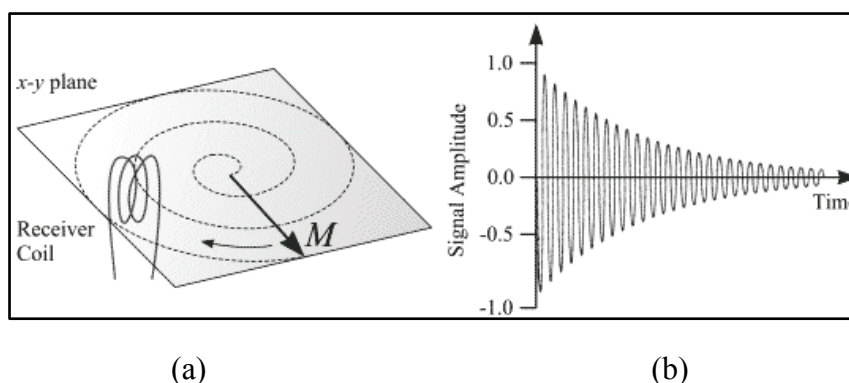


Figure 2.5 (a) After a 90 degrees RF pulse, M lies in the x-y plane and rotates about the z-axis. The component of M in the x-y plane decays over time. An alternating current, shown in Figure (b), is induced in the receiver coil [3].

2.1.3 Spatial Encoding [2]

The appearance of MR images is in terms of brightness or contrast and the digital nature of the image, as pixels or voxels. The image-formation process provides the optimum diagnostic information from an examination, modifying or creating new protocols, recognizing common image artifacts and taking measures to overcome or avoid them. **Anatomy of a pulse sequence:** In MR scanning process, particularly spin echo, may take a long time to acquire, that the progress of the scan involves a loud banging sound from the MR system and that sometimes there is more silence than banging. Each sound is produced by *gradient* pulses applied to interrogate every possible spatial frequency that may contribute to the image. In MR the static magnetic field B_0 is constantly present, the gradients are not. They are applied in a controlled fashion to form an MR *pulse sequence*. MR pulse sequence does a number of things. An MR pulse sequence diagram is a simple means of showing how the RF and gradients are applied. The vertical axis represents amplitude and the horizontal axis is time. Figure 2.6 shows a basic spin echo MR imaging sequence.

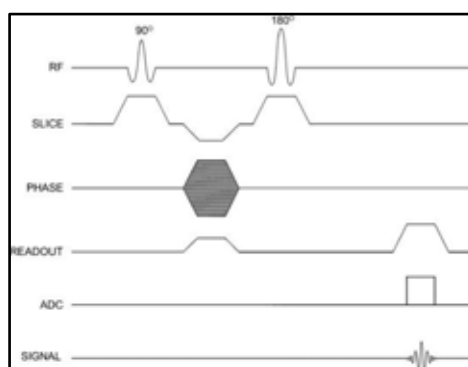


Figure 2.6 Spin echo diagram [4].

First (top line) an RF pulse is applied simultaneously with a slice-selective gradient G_x (line 2). The RF pulse stimulates the MR interactions in tissue which lead to the MR signal. By combining the RF excitation with a gradient the MR interactions are restricted to a two-dimension plane, slab or slice. Any physical gradient G_x , G_y or G_z

or combinations of these can be used for this purpose, allowing us to produce transverse, sagittal or coronal, oblique or double oblique slices. Next, in line 3, *phase encoding* is applied in a direction orthogonal to the slice selection. This encodes the MR signal in the phase encode direction. In line 4, the frequency encoding or readout gradient is applied in the third direction and finally at the bottom line, show the time when the MR signal is measured or *acquired*. (Note) that this is during the frequency encoding gradient until the data or k-space matrix is filled. A time period, TR, occurs between the application of one RF excitation and the next. The total scan time is the product of NSA, N_{PE} and TR;

$$\text{Scan time} = \text{NSA} \times N_{PE} \times \text{TR}$$

where NSA is the number of signal average and N_{PE} the size of the phase encoding matrix. Once all the data are acquired a two-dimensional Fourier transform is applied. This converts the data already encoded as spatial frequencies, into an image reconstruction in MRI. It is generally simpler than in X-ray CT; most of the hard work has been done during the acquisition by the gradients.

Spin echo pulse sequence: The spin echo (SE) sequence is the most commonly used pulse sequence in clinical imaging. The sequence comprises two radiofrequency pulses - the 90 degree pulse that creates the detectable magnetization and the 180 degree pulse that refocuses it at TE. The selection of TE and TR determines resulting image contrast. In T1-weighted images, tissues that have short T1 relaxation times (such as fat) present as bright signal. Tissues with long T1 relaxation times (such as cysts, cerebrospinal fluid and edema) show as dark signal. In T2-weighted images, tissues that have long T2 relaxation times (such as fluids) appear bright.

In cerebral tissue, differences in T1 relaxation times between white and grey matter permit the differentiation of these tissues on heavily T1-weighted images. Proton density-weighted images also allow distinction of white and grey matter, with tissue signal intensities mirroring those obtained on T2-weighted images. In general, T1-weighted images provide excellent anatomic detail, while T2-weighted images are often superior for detecting pathology.

Gradient echo pulse sequence: Gradient echo or Gradient recalled echo (GRE) sequences, which are significantly faster than SE sequences, differ from SE sequences in that there is no 180 degree refocusing RF pulse. In addition, the single RF pulse in a GRE sequence is usually switched on for less time than the 90 degree pulse used in SE sequences. The scan time can be reduced by using a shorter TR, but this is at the expense of the signal to noise ratio (SNR) which drops due to magnetic susceptibility between tissues. At the interface of bone and tissue or air and tissue, there is an apparent loss of signal that is heightened as TE is increased. Therefore it is usually inappropriate to acquire T2-weighted images with the use of GRE sequences. Nevertheless, GRE sequences are widely used for obtaining T1-weighted images for a large number of slices or a volume of tissue in order to keep scanning times to a minimum. GRE sequences are often used to acquire T1-weighted 3D volume data that

can be reformatted to display image sections in any plane. However, the reformatted data will not have the same in-plane resolution as the original images unless the voxel dimensions are the same in all three dimensions.

Inversion recovery: Inversion-recovery is a magnetization preparation technique followed by an imaging sequence of the spin echo type in its standard version. The sequence starts with a 180° RF inversion wave which flips longitudinal magnetization M_z in the opposite direction. Due to longitudinal relaxation, longitudinal magnetization will increase to return to its initial value, passing through null value. To measure the signal, a 90° RF wave is applied to obtain transverse magnetization. The delay between the 180° RF inversion wave and the 90° RF excitation wave is referred to as the inversion time TI. As longitudinal regrowth speed is characterized by relaxation time T1, these sequences are weighted in T1. Inversion-recovery also increases weighting of the associated imaging sequence (spin echo or gradient echo of varying speeds). With this type of sequence; certain tissues have a negative signal. In terms of display, two possibilities exist.

Either signal magnitude (amplitude in relation to 0) used for gray scale display: the more absolute the value of the tissue signal (positive or negative), the stronger it will be.

Or the gray levels will be distributed from the negative signal values to the positive values (with a null signal background that will be gray rather than black): this is the (true) display type. Another property of inversion-recovery sequences is linked to the choice of TI: if a TI is chosen such that the longitudinal magnetization of a tissue is null, the latter cannot emit a signal (absence of transverse magnetization due to the absence of longitudinal magnetization). The inversion-recovery technique thus allows the signal of a given tissue to be suppressed by selecting a TI adapted to the T1 of this tissue. Inversion-recovery can be combined with sequence types other than the standard spin echo. In particular, it can be used with fast spin echo sequences, to save considerable time, as inversion-recovery requires relatively long TR to allow magnetization the time to regrow. Inversion-recovery also serves as magnetization preparation for gradient echo sequences, to weight them in T1.

Ultrafast gradient echo pulse sequence: Ultrafast gradient echo sequences use a small flip angle, a very short TR and optimized k-space filling to reduce acquisition time (to roughly one second per slice). The drawback of a small flip angle and very short TR is poor T1-weighting. To preserve T1 contrast; a 180° inversion pulse prepares magnetization before repetitions of the ultrafast gradient echo imagery sequence. Effective inversion time will correspond to the delay between the inversion pulse and acquisition of the central k-space lines. To obtain T2-weighting, the preparatory pattern is of the spin echo type ($90^\circ - 180^\circ$) so that the ultrafast GE imaging sequence can start with longitudinal magnetization whose amplitude depends on T2. K-space filling can follow variable trajectories (linear, centripetal, and centrifugal) to determine image contrast. Either all the k-space lines are acquired after a single inversion pulse (single shot), or only a group of lines is acquired (segmented filling). The speed of these T1-weighted gradient echo sequences is particularly suited to monitoring Gadolinium bolus arrival in imaging at arterial phase and in T1 high resolution 3D imaging.

Fourier transforms: Josef Fourier was a French mathematician who enjoyed a colorful life spanning science, politics and high society during the time of the Emperor Napoleon Bonaparte. His lasting achievement was the invention of the Fourier transforms a concept which met with much resistance from the scientific establishment of his time, but one which entirely underpins the theory of MR imaging. Fourier's great idea was that any signal or waveform in time could be split up into a series of 'Fourier components' each at a different frequency. For example, the sound of a musical instrument could be described either by the actual pressure waveform it produced in *the time domain*, or by the appropriate magnitude of its constituent frequencies or its *spectrum* in the *frequency domain*. An acoustic signal, such as that produced by a musical instrument, is an example of a one dimensional waveform and when Fourier transformed gives a one-dimension spectrum. In MR we use two- or three-dimensional Fourier transforms. Variables which relate to each other in their respective domains are called Fourier transform pairs. Examples are shown in figure 2.7. One of the key features of the Fourier transform is that 'less is more': if a shape is small in one domain, its transform will be large in the other.

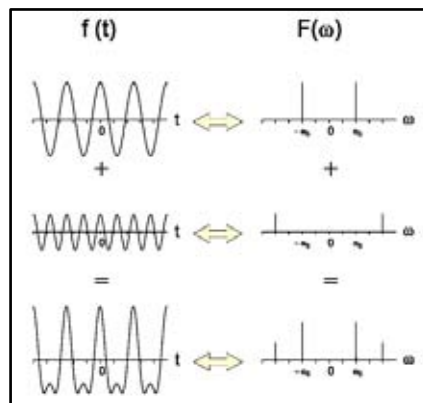


Figure 2.7 The addition property of the Fourier transforms [3]

2.1.4 Imaging Contrast

T1 weighted image: Following termination of an RF pulse, nuclei will dissipate their excess energy as heat to the surrounding environment (or lattice) and revert to their equilibrium position. Realignment of the nuclei along B_0 , through a process known as recovery, leads to a gradual increase in the longitudinal magnetization. The time taken for a nucleus to relax back to its equilibrium state depends on the rate that excess energy is dissipated to the lattice. Let M_0 be the amount of magnetization parallel with B_0 before an RF pulse is applied. Let M_{long} be the z component of M at time t , following a 90 degree pulse at time $t = 0$. It can be shown that the process of equilibrium restoration is described by the equation.

$$M_{\text{long}} = M_0 \times (1 - e^{-t/T_1})$$

Where T1 is the time taken for approximately 63% of the longitudinal magnetization to be restored following a 90 degree pulse.

T2 weighted image: While nuclei dissipate their excess energy to the lattice following an RF pulse, the magnetic moments interact with each other causing a decrease in transverse magnetization. This effect is similar to that produced by magnet inhomogeneity, but on a smaller scale. The decrease in transverse magnetization (which does not involve the emission of energy) is called decay. The rate of decay is described by a time constant, T2*, that is the time it takes for the transverse magnetization to decay to 37% of its original magnitude. T2* characterizes dephasing due to both B0 inhomogeneity and transverse relaxation. Let $M_{0\text{-trans}}$ be the amount of transverse magnetization (M_{x-y}) immediately following an RF pulse. Let M_{trans} be the amount of transverse magnetization at time t, following a 90 degree pulse at time t = 0.

It can be shown that

$$M_{\text{trans}} = M_{0\text{trans}} \times e^{-t/T2^*}$$

In order to obtain signal with a T2 dependence rather than a T2* dependence, a pulse sequence known as the spin-echo has been devised which reduces the effect of B0 inhomogeneity on M_{x-y} . A pulse sequence is an appropriate combination of one or more RF pulses and gradients (see next section) with intervening periods of recovery. A pulse sequence consists of several components, of which the main ones are the repetition time (TR), the echo time (TE), flip angle, the number of excitations (NEX), bandwidth and acquisition matrix.

PD weighted image: Image contrast with spin density weighting relies mainly on differences in the number of magnetizable protons per volume of tissue. At thermal equilibrium, those tissues with a greater spin density exhibit a larger longitudinal magnetization. Very hydrogenous tissues such as lipids and fats have a high spin density compared with protein aqueous soft tissues; aqueous tissues such as CSF also have are relatively high spin density. To minimize the T1 differences of the tissues, relatively long TR is used. This allows significant longitudinal recovery so that the transverse magnetization differences are chiefly those resulting from variations in spin density. Signal amplitude differences are minimized. Spin density-weighted images therefore require a *long TR and a short TE* for the spin echo pulse sequence. Fat and CSF display as a relatively bright signal and a light contrast inversion between white and gray matter occurs. This sequence achieves the highest overall signal and the highest signal-to-noise ratio (SNR) for spin echo imaging; however, the image contrast is relatively poor, and therefore the contrast-to-noise ratio is not necessarily higher than with a T1-or T2-weighted image.

2.1.5 MR equipment [2]

Magnets: The magnet is the main component of the MR system. Due to design constraints the static magnetic field is inherently non uniform and its *homogeneity* is optimized by a process known as shimming where by pieces of steel and/or electrical coils are incorporated into the magnet to improve the uniformity over a given volume. This process is usually performed at system installation; however, many systems give the user limited ability to improve the homogeneity on a per-patient basis during scan set-up. This is particularly important for techniques such as fat suppression or spectroscopy.

A magnet will also generate a magnetic field outside of the patient aperture. Considerable effort is invested in designing magnets whereby the extent of this *fringe field* is minimized. However, for some sites additional magnetic field shielding may be required either for safety reasons or to avoid interference with nearby sensitive electronic components.

Magnetic field strength is measured in Tesla (T). Whole-body magnets have been constructed with field strengths of 0.02-11 T. typical clinical systems operate in the range of 0.2-3 T. Spectroscopy is generally performed at 1.5 T and above. The advantages of higher field strengths are a better SNR and increased chemical shift effects, improving spectral fat suppression and spectroscopy. The improvement in SNR with increasing field strength may be traded for increased spatial resolution, or decreased imaging time.

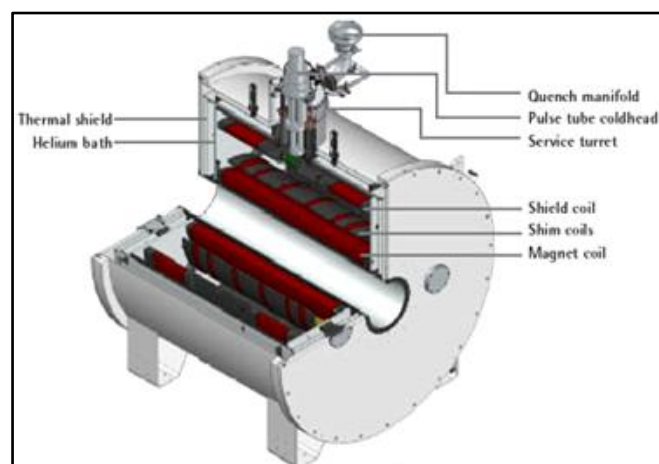


Figure 2.8 Basic magnet component of an MR system.

Gradients: The gradient coils mounted on a cylindrical form just inside the bore of the magnet. In a standard cylindrical magnet, such as a superconducting system, the direction along the bore is termed the z axis, the left-right direction is termed the x axis and the top-bottom direction is termed the y axis. Although the gradients are oriented in the three orthogonal directions, the gradient magnetic fields themselves are parallel to the main magnetic field B_0 . The null point at the center of the gradient coils, and also the center of the magnet, is called the *isocentre*.

The z gradient (G_z) can be generated through the use of a single pair of coils with counter-rotating currents known as a Maxwell pair as shown in figure 2.9. The optimum gradient linearity occurs when the coils are separated by $r\sqrt{3}$, where r is the coil radius. Other designs can generate z gradients with much better radial linearity, e.g. spiral windings with variable pitch along the z axis.

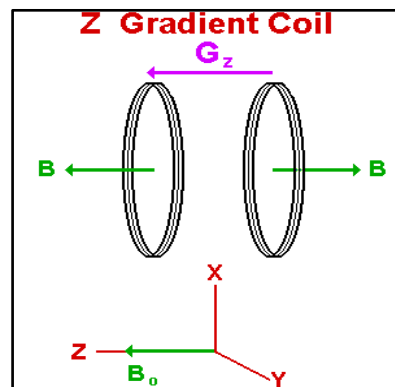


Figure 2.9 Maxwell pair configuration for a longitudinal (Z) gradient field.

The x axis and y axis gradients G_y can be generated using the Golay configuration shown in figure 2.10. Comprising four coils on the surface of the cylindrical former with the currents producing a quadrupolar magnetic field (i.e. one having two North and two South poles). Only the innermost arcs contribute usefully to producing a transverse gradient with the field parallel to B_0 . The G_x gradient can be generated using an identical set of Golay coils rotated through 90° .

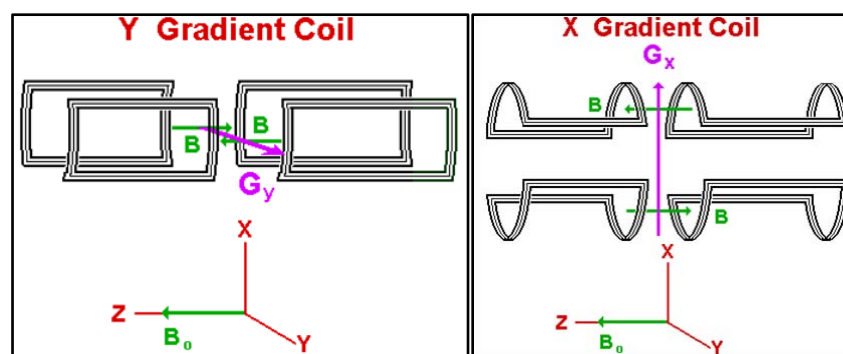


Figure 2.10 Golay coils configuration for transverse (x and y) gradient fields.

Radiofrequency systems: The radiofrequency (RF) system comprises a *transmitter, coil and receiver*. The purpose of the transmitter is to generate suitably shaped pulses of current at the Larmor frequency. When this current is applied to the coil an alternating B_1 field is produced. The coils will also detect the MR signal from the patient. The frequency-encoding process will result in a narrow range of useful frequencies, e.g. ± 32 kHz, centered at the Larmor frequency. It is the function of the receiver to remove, or more correctly demodulate, this ± 32 kHz range of interest from the much higher (Larmor frequency).

The transmitter has to generate RF pulses with appropriate center frequencies, bandwidths, amplitudes and phases in order to excite nuclei within the desired slice or

slabs. The slice position and the strength of the slice select gradient at that location determine the center frequency of the pulse. The bandwidth, or the range of the frequencies within the pulse, controls the slice thickness of the excited slice. The shape and duration of the RF pulse envelope determines the bandwidth. The amplitude of the RF pulse controls how much the magnetization is flipped by the pulse, whilst the phase controls along which axis the magnetization is flipped (in the rotating frame of reference). In modern MRI systems the RF pulse envelope is generated digitally.

The receiver coils maximize signal detection, whilst minimize the noise. Usually the major source of noise is from the patient's tissue (from the Brownian motion of electrolytes). To minimize the noise, and maximize the SNR, it is necessary to minimize the coil dimensions, i.e. the coil's volume should be filled as much as possible by the sample. A compromise needs to be made between adequate RF homogeneity and SNR. There are two types of receiver coil: volume and surface. Volume coils completely encompass the anatomy of interest and are often combined transmit/receive coil. Surface coils are generally receiver only, due to their inhomogeneous reception field. They are however, as their name suggests, good for detecting signal near the surface of the patient.

Receiver coils can also operate in quadrature. During reception the signals from the two-quadrature modes add constructively, whilst the noise from each is uncorrelated, i.e. it „averages out“, resulting in a $\sqrt{2}$ improvement in SNR over a comparable linear coil.

2.1.6 MRI Artifacts [6]

Artifact in MR images refer to pixels that do not faithfully represent the anatomy being studied. The general appearance of the images is that the underlying anatomy is visualized but spurious signal are present that do not correspond to actual tissue at that location. The artifact may or may not be easily discernible from normal anatomy, particularly if they are of low intensity, and may or may not be reproducible.

Phase sampling artifact: Aliasing or wrap-around corresponds to overlapping on the opposite side of the image of signals outside of the FOV. It is caused by a corruption in the spatial encoding of objects outside the FOV which cannot be distinguished from objects inside the FOV. It results in a spatial mismatching to the opposite side of the image. Although this artifact can occur in both the frequency and the phase-encode directions, it is actually only an issue in the phase-encode direction.

The range of meaningful phase values is -180° to $+180^\circ$. It can be represented as the angle corresponding to a position on a circle. A phase of 180° is equivalent to -180° , 200° is equivalent to -160° ($200^\circ - 360^\circ$), 220° is equivalent to -140° etc... Phase-encoding consists in modifying the phase of spins in a direction of the slice plane. The phase shifts, ranging from -180° and $+180^\circ$ at the first encoding step, are assigned to cover the FOV. The next phase-encoding steps use larger ranges which are always a multiple of $-180^\circ / +180^\circ$. If an object extends outside the FOV, it will experience a phase shift (because the phase-encoding gradient is applied on the whole

body) but its value will be outside the range. For example, if we consider the first encoding step, the phase shift will be less than -180° or greater than $+180^\circ$. Therefore, these values outside the range will be spatially mismapped (200° is equivalent to -160° ...): the reconstruction will produce images with an overlapping of the objects outside the FOV on the opposite side of the image.

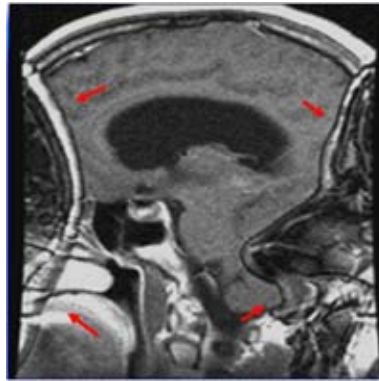


Figure 2.11 Phase sampling/phase wrap artifact

Susceptibility and Metal artifacts: Magnetic susceptibility is defined as the extent to which any material becomes temporarily magnetized when it is placed in a large magnetic field. Among the body tissue, bone has the lowest susceptibility, similar to air, most tissues have mid-range susceptibility, while iron-containing molecules such as hemoglobin and blood breakdown products have the highest. At the boundaries between these tissues, the slightly different magnetic fields within the tissues create micro-gradients which speed up the dephasing between protons on either side of the boundary. The phase change, $\Delta\omega$, caused by susceptibility is given by the equation.

$$\Delta\omega = \gamma \times G_i \times \Delta r \times TE$$

Where γ is the gyromagnetic ratio, G_i is the internal magnetic field gradient, and Δr is the voxel size. This equation shows that susceptibility artifacts are worst with large voxels and at long TEs, and can be minimized by reducing TE or increasing the resolution. Often there is not just one simple boundary but many tiny boundaries on a microscopic level, for example in signal of susceptibility artifacts.

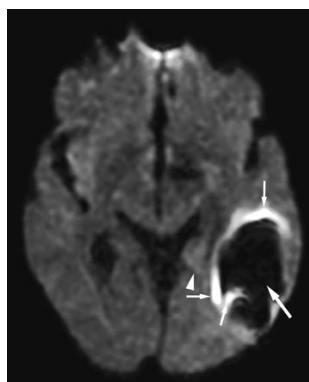


Figure 2.12 Susceptibility artifact

Zipper artifact: The zipper artifact is the RF breakthrough, is probably the most common equipment artifact. It appears as a line of alternating light and dark pixels sometimes two or three pixels wide, extending across the image in the phase-encode direction. Occasionally there will be multiple ghost zippers, regularly spaced across the image, but usually there is just one, most often in the center of the FOV.

The cause of the zipper is external RF radiation finding its way into the magnet room and being picked up by the imaging coils or due to a break in the RF screened room – the metal shield built into the walls, floor and ceiling of the scan room. In this case, the artifact will be present on all images and the manufacturer’s engineers should be called to investigate the problem.

A more common cause is anesthetic monitoring equipment, especially if it relies on metallic leads or mains leads going through the waveguides into the scan room. The leads pick up RF waves from the environment and carry them through the Faraday cage, then transmitting them into the room where they are picked up by RF imaging coils. Even if there are no leads going through the waveguides, some pulse oximeters use radiofrequency noise-reduction processing, which may also be picked up by the imaging coils if the equipment has defective RF shielding. These problems can be particularly difficult to track down. Although it is more expensive, all monitoring equipment used should be the specially MRI- compatible type – it saves a lot of heartache over zipper artifact.

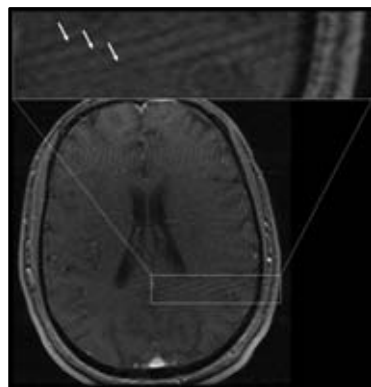


Figure 2.13 Zipper artifacts [7]

Truncations artifact: Truncation artifact also referred to as “Gibbs ringing” or edge-ring artifact may appear in many ways: “ringing” which involves alternating light and dark bands; edge enhancement between areas of low and high signal intensity; and distortion of the size and shape of structures. Truncation artifacts can be diminished by several mechanisms. Decreasing the size of image pixels relative to the size of geometrical structures in the image achieved by decreasing the FOV or increasing the matrix size, reduces the representation of the artifact on the final image. However, increasing the matrix size increasing scan time and decreases the signal-to noise ratio. Alternatively, decreasing the FOV may cause aliasing. These detrimental effects on image quality must be weighed against the possible benefit from removing the truncation artifact. Use of a filter that discards artifactual frequencies is another means of decreasing truncation artifact.

The data acquired in k space for an MR image represents a finite amount of digital information due the fact that the MR signal is sampled over a limited period of time. This inevitably leaves out waveforms, occurs then on a truncated amount of data, this result in deviation from the ideal signal intensity for any given image pixel. This phenomenon causes artifacts in particular in areas where signal changes abruptly, because Fourier transforms analysis poorly accounts for such changes.

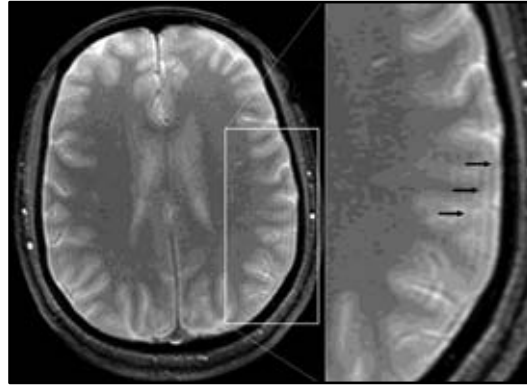


Figure 2.14 Truncation artifacts [7]

2.1.7 MRI 3 Tesla and Susceptibility artifact

Magnetic resonance imaging (MRI) systems working at field strength, B_0 , of 3 Tesla have become more and more frequent use in recent years. As an increasing number of radiological sites, 3-Tesla MRI starts to play the same role for clinical imaging that was occupied by 1.5-Tesla systems for about the last 10 years. The main motivation for the transition from 1.5-Tesla to 3-Tesla MRI systems is the improved signal to-noise ratio (SNR), which is approximately proportional to the field strength, B_0 ; thus, under ideal conditions and with optimized acquisition techniques a doubled SNR can be expected at 3 Tesla in comparison to 1.5 Tesla. The growing availability of 3-Tesla MRI systems is for instance demonstrated by the number of publications on 3-Tesla MRI listed in the Medline database, which increased from around 30 in the year 2000 to more than 400 in 2006. Typical applications included functional MRI or spectroscopy studies of the brain, which were performed with optimized protocols and under attendance of specialized engineers or physicists. Today, the availability of 3-Tesla MRI systems has substantially broadened and these systems are applied for imaging of all anatomical areas including e.g. musculoskeletal, abdominal, cardiac, angiographic and whole-body imaging. This development leads to an increasing diversity of applied pulse sequences and protocols, which are not always fully optimized for 3-Tesla MRI. Consequently, the radiologist or technician working with such 3-Tesla protocols will comparatively frequently be confronted with image artifacts related to 3-Tesla MRI.

B_0 inhomogeneity and susceptibility effects: B_0 defines the main static field of the MR system. A well-shimmed 3-T whole-body MR system can provide field homogeneity specifications that are comparable with or even improved over those of 1.5-T systems. One vendor reports a 0.25 ppm root mean square voltage error, or

V_{RMS} , at 40-cm diameter of sensitive volume, or DSV, and 1 ppm V_{RMS} at 50-cm DSV at 3 T (Siemens Medical Solutions, Erlangen, Germany). Other vendors offer 0.5 ppm V_{RMS} or less at 40-cm DSV at 3 T (GE Healthcare, Waukesha, Wisconsin, USA) and Philips Medical Systems, Best, the Netherlands [Romhild Hoogeveen, personal communication].

Once a subject is placed into the bore of the magnet, differences in magnetic susceptibility of tissues lead to local alterations of the magnetic field. Susceptibility effects are larger at 3 T than 1.5 T because of a linear dependence of the magnetization on the field strength. There are several consequences of this increased susceptibility. The shortened $T2^*$ relaxation times that result from local field distortions cause greater signal loss at a given TE at 3 T than at 1.5 T. Given that spatial localization relies on gradient-induced frequency and phase encoding, susceptibility-induced field alterations also lead to image distortions. For some applications such as functional MR imaging of the brain, where the blood oxygenation level-dependent, or BOLD, effect relies on the susceptibility effects of deoxyhemoglobin, this greater sensitivity at 3 T is highly desirable. Susceptibility-weighted imaging of the brain, and even some abdominal imaging applications, may benefit from greater susceptibility. For example, improved sensitivity to iron deposition in the liver and other organs may be useful in the detection of diseases such as hemochromatosis. The signal-to-noise and contrast-to-noise effects of iron-based contrast agents depend on the sequences and doses and are the subject of active investigation.

However, for MRI applications, greater susceptibility creates undesirable image distortions and signal loss for example, in regions such as bowel-gas and cardiac-lung interfaces and around implanted metallic clips or prostheses (Figure 2.15).

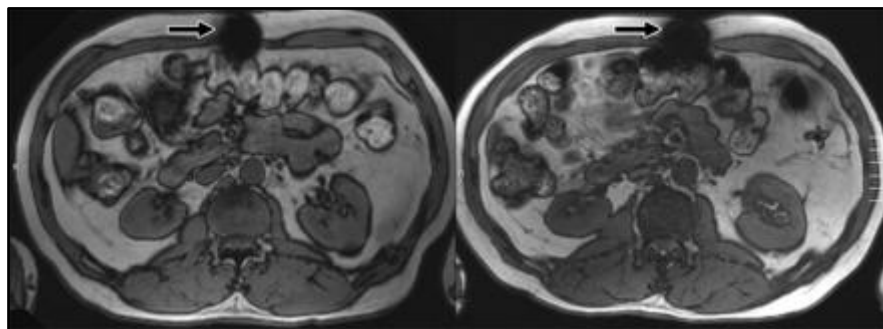


Figure 2.15 Transverse T1-weighted gradient-echo MR images (repetition time, 167 msec; flip angle, 90°) illustrate greater susceptibility effects (arrow) associated with anterior abdominal wall surgical clips at (right) 3 T (TE, 1.58 msec) compared with at (left) 1.5 T (TE, 2.38 msec) despite the considerably shorter TE used in the same subject[8].

2.1.8 Introduction of Neuro endovascular Intervention

Endovascular coiling is a procedure performed to block blood flow into an aneurysm (a vascular pouch represent weakened area in the wall of an artery). Preventing blood flow into an aneurysm helps to keep the aneurysm from rupturing (bursting). Coiling does not require a surgical procedure. Rather, a catheter is inserted into an artery in the groin, and then advanced into the affected artery in the brain. X-rays are used to guide the catheter into the artery. Coiling may also be used to treat a condition called arteriovenous fistula, or AVF. An AVF is an abnormal connection between an artery and a vein that may occur in the brain, spinal cord, or elsewhere in the body. The coils used in this procedure are made of soft platinum metal, shape like a spring. These coils are very small and thin, ranging in size from about twice the width of a human hair to less than one hair's width.

Aneurysms may be treated in different ways, depending on the type of aneurysm, where it is located in the brain, and the patient's medical condition. The standard surgical method for treating a cerebral aneurysm is called aneurysm clipping. In this procedure, a small metal clip is used to stop blood flow into the aneurysm, after an opening has been made in the skull to reach the aneurysm in the brain. The clip looks much like a clothespin. It is placed on the neck (opening) of the aneurysm to obstruct the flow of blood, and remains inside the brain. Coiling is a newer procedure that has become available since the mid-1990. Coiling has advantages over surgical aneurysm clipping, because it does not involve opening the skull, and hospitalization time and recovery time are often shorter. However, not everyone with a cerebral aneurysm or AVM is suitable for a coiling procedure [9].



Figure 2.16 Coil procedures for cerebral Aneurysm [9]

Noninvasive Imaging of Treated Cerebral Aneurysms: Regular imaging follow-up of patients with intracranial aneurysms treated with neurovascular coils is necessary because of the risk of aneurysm reconfiguration (i.e., coil compaction and/or growth of a residual aneurysm neck or body remnant) with time. Within the techniques available for monitoring the results of embolization therapy, MR angiography (MRA) has emerged as the technique of choice at most institutions. Advantages over conventional digital subtraction angiography (DSA) include minimal invasiveness with no associated risk of neurologic complications, reduced patient discomfort and inconvenience, greater cost savings, and no exposure to ionizing radiation or potentially nephrotoxic iodinated contrast media. An alternative

minimally invasive procedure is CT angiography (CTA). However, whereas this technique has proved useful for aneurysm detection, limitations to its use for follow-up of coiled aneurysms include streak and other coil-related artifacts. Moreover, CTA also requires exposure to ionizing radiation and iodinated contrast media, which may be undesirable if repeat follow-up examinations are required.

2.2 Review of Related Literature

Hennemeyer C.T, Wicklow K., Feinberg D.A, et al [10]. In Vitro Evaluation of Platinum Guglielmi Detachable Coils at 3 T with a Porcine Model: Safety Issues and Artifacts. Radiology 219 (2001):732–737. Evaluated safety-related issues and imaging artifacts of Guglielmi detachable coils in vitro with 3-T magnetic resonance (MR) imaging. Two aneurysm models were constructed: one from porcine carotid artery and the other from a pharmaceutical capsule. Both were filled with Guglielmi detachable coils. The models were tested with a 3-T MR imager for heating, deflection, and imaging artifact. Testing for heating and deflection was performed (a) at static points both inside and outside the bore, (b) during movement into the imager, and (c) during clinical imaging sequences.

The results showed no change in temperature measured during movement into the imager bore or at different points within the bore. No differences in heating from radio-frequency energy were found between aneurysm models and controls. Similarly, no evidence of deflection of the coil mass (capsule model) was found. Minor susceptibility artifacts were found in the readout direction during gradient-echo sequences. Magnetic field mapping showed no induced field inhomogeneity.

Walker M.T, Tsai J., Parish T., et al [11]. MR Angiographic Evaluation of Platinum Coil packs at 1.5T and 3T: An in vitro assessment of Artifact Production. AJNR Am J Neuroradiol. 26(2005):848-853. Studied of the susceptibility artifact from platinum coil packs impair the visibility of perianeurysmal soft tissues at conventional 3D time-of-flight MR angiography. These artifacts limit the evaluation for residual-recurrent aneurysm and parent vessel stenosis. The purpose of this study is to assess quantitatively the effect of decreasing the echo time on artifact production at different field strengths and coil pack densities.

The results showed *volume measurement data* significantly more volume artifact produced at 3T than at 1.5T. At both field strengths, the more densely packed aneurysm produced more artifact than the less densely packed aneurysm; however, this was statistically significant only at 3T. There was a significant effect on volume artifact as a function of sequence (TE) for both the 1.5T and 3T. At both field strengths, the longer TE sequences produced the most artifacts, with both of these sequences differing significantly from all the others.

Diameter Measurement Data The 3T groups produced artifacts with significantly greater diameters than the 1.5T groups. The diameters were greatest for the CC plane Sequence parameter changes yielded a statistically significant effect on

artifact diameter measurements, with CC yielding the highest diameters. For all three planes, the longer TE sequences yielded significantly higher artifact diameter than any other sequence.

Lee M.J, Kim S., Lee S.A, et al [12]. Overcoming Artifacts from Metallic Orthopedic Implants at High-Field-Strength MR Imaging and Multidetector CT. RadioGraphics 27 (2007):791–803. Evaluated magnetic resonance (MR) imaging and multidetector computed tomography (MDCT) artifacts arising from metallic orthopedic hardware, an obstacle to obtaining optimal images. Factors that affect artifacts on MR images include the composition of the metallic hardware, the orientation of the hardware in relation to the direction of the main magnetic field, the strength of the magnetic field, the pulse sequence type, and other MR imaging parameters (mainly voxel size, determined by the field of view, image matrix, section thickness, and echo train length). At MDCT, the factors that affect artifacts include the composition of the hardware, orientation of the hardware, acquisition parameters, and reconstruction parameters. A comparison of images obtained with different hardware and different acquisition and reconstruction parameters facilitates an understanding of methods for reducing or overcoming artifacts related to metallic implants.

The result shows reduce metal-related artifacts at MR imaging, orthopedic hardware should be positioned to parallel as closely as possible the direction of the main magnetic field. With respect to hardware composition, a titanium alloy produces less severe artifacts than does stainless steel. The fast SE pulse sequence is the best MR imaging sequence for artifact reduction, and the GRE sequence is the least beneficial. For purposes of suppressing the signal from fat while avoiding severe metal related artifacts, the STIR pulse sequence is preferable to frequency-selective fat saturation. Use of lower magnetic field strength is desirable; however, if a currently available clinical MR imaging system with a high-field-strength magnet is used, the imaging parameters chosen (e.g., small field of view, high-resolution image matrix, thin sections, increased echo train length, and higher gradient strength for small voxel sizes) may help reduce metal-related artifacts.

Shellock F.G, [13] Metallic neurosurgical implants: evaluation of magnetic field interactions, heating, and artifacts at 1.5-Tesla. Magn Reson Imaging 14(2001): 295-9, evaluated the magnetic resonance imaging (MRI) safety aspects for seven different metallic neurosurgical implants in association with the 1.5-T MR environment. In vitro testing was performed using previously-described techniques for the evaluation of magnetic field interactions (deflection angle and torque), heating, and artifacts (using T1-weighted, spin-echo and gradient-echo pulse sequences). None of the metallic implants displayed interactions with the magnetic field. Artifacts were relatively minor. The lack of magnetic field interactions and negligible heating indicate that MR procedures may be conducted safely in patients with these neurosurgical implants using MR systems with static magnetic fields of 1.5-T or less.

The resulted artifact grades for the two different pulse sequences and planes of imaging. In general, the artifacts were relatively small, localized signal voids insofar as they closely resembled the size and shape of the implants. The GRE pulse sequence produced a slightly larger artifact than the T1- weighted spin-echo pulse sequence for the implants.

Farrelly C., Davarpanah A., Brennan S., et al [14], Imaging of Soft Tissues Adjacent to Orthopedic Hardware: Comparison of 3-T and 1.5-T MRI. AJR 94(2010): 60-64. Compare metal artifact reduction techniques at 1.5-T and 3-T MRI. A titanium plate with steel screws was placed in a freshly harvested pig leg. The leg was imaged with 1.5-T and 3-T MRI. A T2-weighted turbo spin-echo sequence was used with echo-train lengths of 8, 16, 32, and 64 and a constant readout bandwidth of 31.2 kHz. The images were compared qualitatively, and the optimal echo train length was selected. Images were acquired at the optimal echo-train length with four different readout bandwidths. Artifact was measured quantitatively, and image quality was ranked qualitatively. The qualitatively best image acquired at 1.5 T was compared with the qualitatively highest-ranked image acquired at 3 T.

The results showed at both 1.5 T and 3 T, optimal images of equal quality were produced at echo train lengths of 8 and 16. At higher readout bandwidths, there was quantitatively less artifact. The qualitatively best images were acquired at a readout bandwidth of 31.2 kHz at 1.5 T and 62.5 kHz at 3 T. The optimal image at 3 T was qualitatively superior to that at 1.5 T.

Kakeda S., Korogi Y., Hiai Y., et al [15], MRA of intracranial aneurysms embolized with platinum coils: a vascular phantom study at 1.5T and 3T. Magn Reson Imaging 28(2008): 13-20, Studied the influence of matrix and echo time (TE) of three-dimensional time-of-flight (3D TOF) magnetic resonance angiography (MRA) on the depiction of residual flow in aneurysms embolized with platinum coils at 1.5T and 3T. A simulated intracranial aneurysm of the vascular phantom was loosely packed to maintain the patency of some residual aneurysmal lumen with platinum coils and connected to an electromagnetic flow pump with pulsatile flow. MRAs were obtained altering the matrix and TE of 3D TOF sequences at 1.5T and 3T.

The result showed the increased spatial resolution and the shorter TE offered better image quality at 3T. For the depiction of an aneurysm remnant, the high-spatial-resolution 3T MRA (matrix size of 384 x 224 and 512 x 256) with a short TE of $< \text{or} = 3.3$ msec were superior to the 1.5T MRA obtained with any sequences.

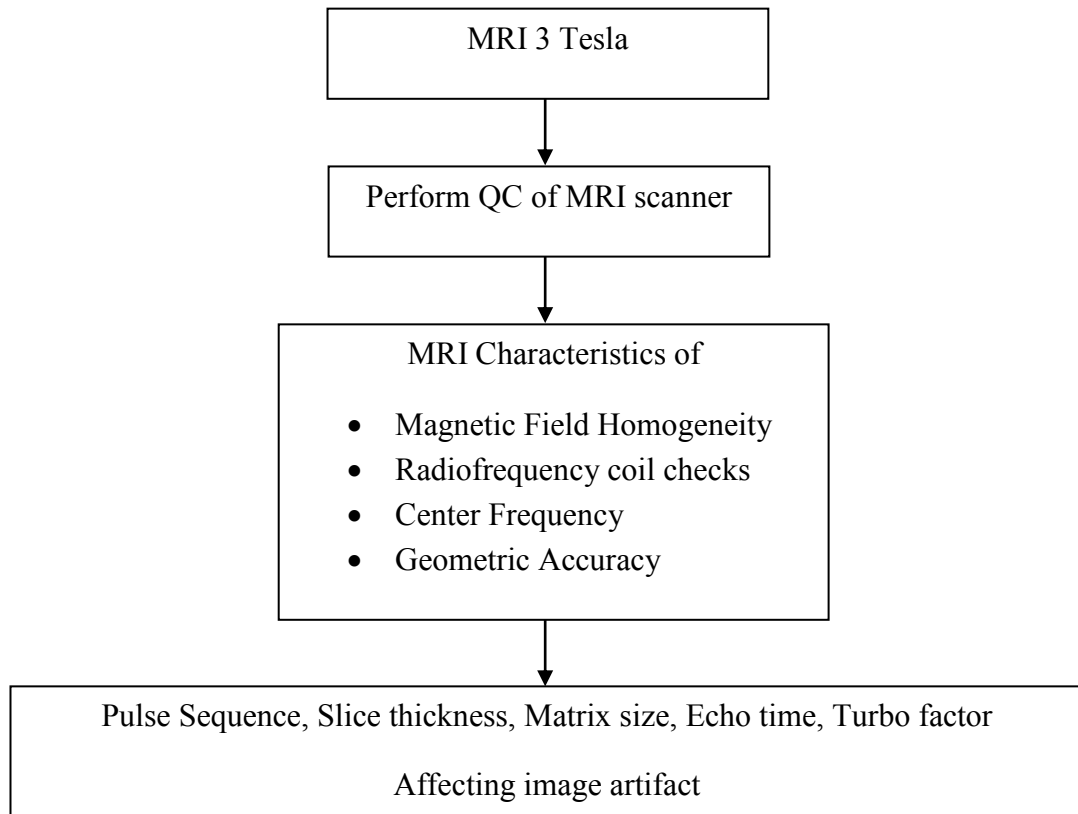
CHAPTER III

RESEARCH METHODOLOGY

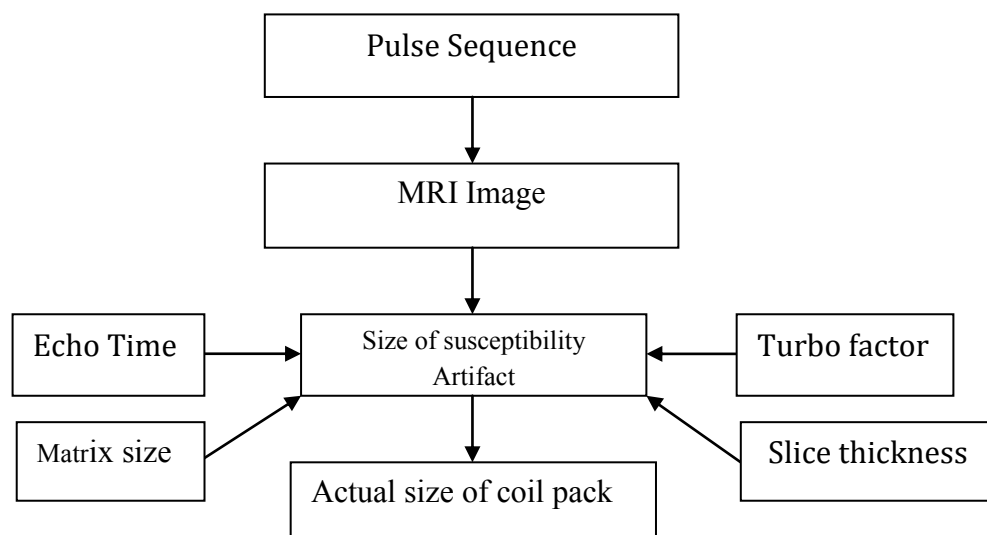
3.1 Research Design

This study is descriptive experimental research.

3.2 Research Design Model



3.3 Conceptual Framework



3.4 Research Questions

3.4.1 Primary Question

What pulse sequences reduce susceptibility artifact in 3 Tesla MRI?

3.5 Materials

3.5.1 MRI 3.0 Tesla, Philips Medical System: Achieva



Figure 3.1 MRI 3.0 Tesla (Philips Medical System: Achieva, Best, Netherland)

MRI 3.0 Tesla, at Advanced Diagnostic Imaging and Image-Guided Minimal Invasive Therapy Center (AIMC), Ramathibodi Hospital has been installed in 2006.

3.5.2 8-Channel SENSE Head coil



Figure 3.2 8-Channel SENSE Head coil

The 8 channel SENSE head coil is domed design which produces exceptional signal-to-noise ratio improvements at 3.0T. Uniformity and coverage makes this coil ideal for standard head imaging or as a high performance coil for brain procedures. The sensitive volume is 24cm^3 in the S/I direction with increase SNR throughout.

3.5.3 Endo neurovascular coils



Figure 3.3 Endo neurovascular coil

Detachable platinum coils are used to occlude intracranial aneurysms; significantly reducing the incidences of aneurysm rupture or re-rupture. The coils are made of platinum that can be visible via X-ray and be flexible enough to conform to the aneurysm shape. The coil is attached to a delivery wire and fed through a micro catheter into the aneurysm. The delivery wire allows the physician to reposition or withdraw the coil to ensure ideal placement. Once properly positioned within the aneurysm, the coil is detached from the delivery wire using an electrolytic detachment process. Five different coils [Trufill coils (3 x 30, 4x30, 30x300 and 40x30 mm, Cordis, Miami, FL, U.S.A.)] were deployed in three tubes.

3.5.4 ACR MRI phantom



Figure 3.4 ACR MRI phantoms

The ACR MRI accreditation phantom is constructed of acrylic plastic, glass, and silicone rubber. Ferromagnetic materials have been excluded. The phantom is a cylinder of 20.4 cm diameter by 16.5 cm length. Internal dimensions are 19.0 cm diameter by 15.0 cm length. The compact design allows placement in axial coronal, or sagittal orientation in almost all MRI head coils. Thus, tests can be conducted in all three major planes. There is a reference line down one side of the phantom.

3.5.5 Vascular phantom

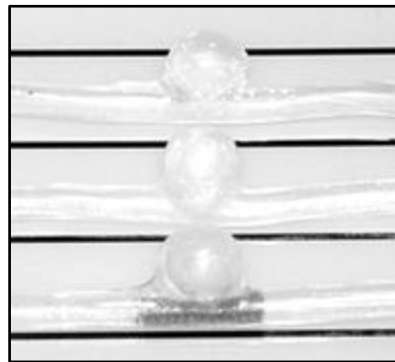


Figure 3.5 Silicone tube.

A silicone tube with inner diameter of 2 and 6 mm was deployed aneurysm in three tubes. The silicone tubes were filled with normal saline solution. This vascular phantom was placed in the center of the sense head coil with the longitudinal axis of the silicone tube roughly parallel to the main magnetic field.

3.5.6 Advantage Workstation



Figure 3.6 Advantage workstation program

Advantage Windows include a consistent 3D environment for routine and advanced post-processing. Workflow optimization is achieved with post-fetch, dynamic load, auto-contour and multi-session. The multimodality management with new Integrated Registration, Volume Viewer for MR and Interventional strengthens this unique post-processing platform with new clinical applications covering all care areas and modalities [16]

- Volume viewer
- Maximum intensity imaging
- 3D Volume rendering
- 3D Multi-planar rendering

- CT-MR perfusion analysis
- Cardiac analysis

3.5.7 SPSS program

SPSS (originally, Statistical Package for the Social Sciences) is a computer program used for statistical analysis. SPSS is among the most widely used programs for statistical analysis in social science. It is used by market researchers, health researchers, survey companies, government, education researchers, marketing organizations and others. In addition to statistical analysis, data management (case selection, file reshaping, creating derived data) and data documentation (a metadata dictionary is stored in the data file) are features of the base software. Statistics included in the base software.

- Descriptive statistics: Cross tabulation, Frequencies, Descriptive, Explore, Descriptive Ratio Statistics
- Bivariate statistics: Means, t-test, ANOVA, Correlation (bivariate, partial, distances), Nonparametric tests
- Prediction for numerical outcomes: Linear regression

SPSS program was used to calculation the ANOVA for assessment analysis of variance three structures of image artifact and coils packs.

3.6 Methods

3.6.1 QC for MRI scanner

The quality control of MRI 3.0 Tesla was performed following the ACR manual (2004) [17] and AAPM report No.100 (2010) [18]. The specific image parameters are: high contrast resolution, low contrast sensitivity, slice thickness, slice position, geometric distortion and image uniformity.

3.6.2 The characteristics of Susceptibility artifact of Endovascular Coils

The characteristics of susceptibility artifact of endovascular coil consists of an area of zero signal and very high intensity rim on edges image .An aneurysm phantom with coils packs diameter 3.0x5.0x5.0, 6.0x6.0x9.8 and 7.6x6.5x9.0 mm were scanned by 3 Tesla MRI equipment.

3.6.2.1 MRI Scanning techniques

- The aneurysm phantom was placed at the center of the 8 elements sense head coil.
- The three orthogonal plane 2D Pulse sequence Spin Echo, Fast Spin Echo, Inversion Recovery and Fast Gradient Echo were obtained from the parameters as shown in Table 3.1.

Table 3.1 The MRI scanning technique at MRI 3.0 T.

Parameter	Inversion Recovery	Spin Echo	Fast Spin Echo	Fast Gradient Echo
TR(ms)	11000	700	4000	107
TE(ms)	125	15	80	4.6
TSE Factor	-	-		-
TI(ms)	2800	-	-	-
FOV(mm)	180	180	180	180
Matrix	Varies	Varies	Varies	Varies
TH(mm)	Varies	Varies	Varies	Varies
Gap(mm)	0.0	0.0	0.0	0.0
BW(Hz)	Varies	Varies	Varies	Varies

TR: time repetition, TE: time echo, TSE Factor: turbo spin echo factor, TI: time inversion recovery, FOV: field of view, Matrix: matrix size, TH: slice thickness, Gap: slice gap, BW: bandwidth.

3.6.3 Quantitative assessment

The three Orthogonal plane 2D Pulse sequence Spin Echo, Fast Spin Echo, Inversion Recovery and Fast Gradient Echo image at coils packs diameter 3, 6 and 10 mm were evaluated to obtain the diameter and volume measurement by placing diameter measurement tool and ROI at the edge of image. The diameter and volume were used to calculate area of artifact.

3.6.4 Assessment of the Neuro endovascular coils packs and Susceptibility artifact and measurement of image artifact for MRI 3.0 Tesla.

The purpose of this study is to determine the susceptibility artifact over actual size Neuro Endovascular coils packs of MRI 3.0 T. This study is followed with protocol MRI and MRA cerebral aneurysm case. However, the diagnostic requirement for MRI and MRA imaging is not only this series group but also the Echo Planar Imaging and Susceptibility Weight Image.

3.7 Data analysis

3.7.1 Image Evaluation

This research is a descriptive study which phantom was used to the MR Imaging examination at 3.0 Tesla.

3.7.2 Diameter and Volume measurement (Quantitative image analysis).

The quantitative image is analyzed by create a line to measure the distance at the edge of the image and region of interest around the edges of the artifact. The distance and area in these regions of interest were used to calculate the signal loss volume and overestimation factor of the artifact.

3.8 Sample size determination

The image quality from both field strengths MRI scan was determined the sample size between two related groups and calculated as following.

- 3 Aneurysm sizes
- 3 Number of scan
- 3 Parameters (TE and Turbo factor)
- 4 Pulse sequence

3.9 Statistical analysis

The signal intensity loss volume data and the overestimation data were analyzed with an analysis of variance (ANOVA) and mean. The diameter data in the three orthogonal planes (Axial, Coronal, Sagittal) were also analyzed with repeated measures ANOVA tests. The effects of parameter changes, coils packs density were analyzed. The null hypothesis was rejected at $P \leq 0.05$.

3.10 Outcome measurement

Phantom study

Independent variables: Number of sampling average (NSA), Field of view (FOV), Time repetition (TR), Flip angle and Variable bandwidth.

Dependent variables: Pulse sequence, Matrix size, Slice thickness, Time to echo (TE) and Turbo factor.

3.11 Expected benefits

The effect of pulse sequence to the susceptibility artifact of the neuro endovascular coils. Magnetic Resonance Imaging parameters are matrix size, slice thickness; echo time and turbo factor to minimal susceptibility artifact the follow-up treatment of patients with cerebral aneurysm neuro endovascular coils on the image of Magnetic Resonance Imaging 3 Tesla. Optimized protocols for Magnetic Resonance Imaging of the endovascular coil embolization at 3 Tesla MRI is obtained.

3.12 Ethical consideration

Most parts were performed in phantom to investigate the physical characteristics of susceptibility artifact. The ethical had been approved by the Ethics Committee, Faculty of Medicine, Chulalongkorn University.

CHAPTER IV

RESULTS

4.1 Quality control of MRI scanners

The quality control of MRI 3.0 Tesla, was performed by following the ACR Phantom manual (2008) [17], AAPM report No.100 (2010) [18]. The results of image uniformity, high contrast resolution, low contrast sensitivity, slice thickness, slice position/separation and geometric distortion are shown in Appendix B. The report of MRI system performance test is shown in Table 4.1

Table 4.1 REPORT OF MRI SYSTEM 3.0 T PERFORMANCE TEST

LOCATION	Sirikit Medical Center Building, Floor 2 Ramathibodi Hospital
DATE	June 16, 2011
MANUFACTURER	Philips Medical Systems
MODEL	Achieva 3.0 Tesla
SOFTWARE VERSION	Examcard version 2.6.3
Image Intensity Uniformity	pass
Percent-Signal Ghosting	pass
High Contrast Resolution	pass
Low Contrast Sensitivity	pass
Slice Thickness accuracy	pass
Geometric Distortion	pass
Slice Position accuracy	pass

4.2 Diameter Measurement Data

The diameter measurements were calculated on the basis of the measured artifact diameters compared with actual coil pack diameter measurement.

4.2.1 Evaluation of the artifact diameter.

A. Variation of pulse sequence

The three orthogonal planes, an actual size of coils packs dimension is 5.0x2.0x5.0, 5.6x5.6x9.8 and 7.6x6.5x9.0 mm (maximum Width x Length x Height). For four pulse sequence MRI 2D images are displayed with the study of the signal loss due to coil induced susceptibility artifact affected by the matrix size of 256x192, 256x256, 512x256 and slice thickness of 3, 5, 7 mm at MRI 3.0 T. The pulse sequence is Spin Echo, Fast Spin Echo, Inversion Recovery and Fast Gradient Echo. The table of percent error from diameter measurement is shown in Table 4.1-4.3.

Table 4.2 Percent error in pulse sequence of signal loss due to coil-induced in susceptibility artifact when compared to actual size of coils pack dimension of 2.0x2.0x5.0 mm diameter of (A/C/S), A = Axial, C = Coronal, S = Sagittal at different matrix No.

Matrix No/Slice thickness	Percent error			
	Spin Echo	Fast Spin Echo	Inversion Recovery	Fast Gradient Echo
256x192/3	33.25	32.5	28.25	75
256x256/3	25.75	25	25.75	75
512x256/3	20	9	21.5	64
256x192/5	21.5	35	32.5	80
256x256/5	21.5	22.5	35	77.5
512x256/5	37	36.3	20	80
256x192/7	44	25	35	81.5
256x256/7	47.5	14	32.5	80
512x256/7	21.5	11.5	24	77.5

From Table 4.2, the smallest percent error of 9 was obtained at fast spin echo for any parameter MRI images at matrix 512x256, slice thickness 3 mm.

Table 4.3 Percent error in pulse sequence of signal loss due to coil-induced susceptibility artifact actual size of coil pack dimension 5.6x5.6x9.8 mm; (A/C/S), A = Axial, C = Coronal, S = Sagittal

Matrix size/Slice thickness	Percent error			
	Spin Echo	Fast Spin Echo	Inversion Recovery	Fast Gradient Echo
256x192/3	44.71	19.42	22.85	93.71
256x256/3	37.14	18.57	17.57	88
512x256/3	26.57	12.28	14.28	104
256x192/5	58	39.42	36.14	92.28
256x256/5	53.28	36.57	32.85	89
512x256/5	32.85	30.85	26.14	74.71
256x192/7	58.57	44.28	47.14	110.42
256x256/7	48	36.14	31.85	87.57
512x256/7	37.14	25.71	26.14	83.28

From Table 4.3, the smallest percent error of 12.28 was obtained at fast spin at matrix 512x256, slice thickness 3 mm.

Table 4.4 Percent error in pulse sequence of signal loss due to coil-induced susceptibility artifact actual size of coil pack dimension 7.6x6.5x9.0 mm; (A/C/S) A = Axial, C = Coronal, S = Sagittal

Matrix size/Slice thickness	Percent error			
	Spin Echo	Fast Spin Echo	Inversion Recovery	Fast Gradient Echo
256x192/3	35.84	23.37	12.46	46.23
256x256/3	33.76	15.58	11.68	36.36
512x256/3	24.67	5.19	2.98	28.96
256x192/5	38.05	18.57	22.85	57.14
256x256/5	35.45	15.06	15.58	47.14
512x256/5	23.37	12.07	5.58	40.25
256x192/7	53.63	27.27	29.35	65.71
256x256/7	41.03	14.67	18.57	49.74
512x256/7	25.06	9.87	10.38	46.75

From the Table 4.4, the smallest percent error of 5.9 obtained at fast spin echo at matrix 512x256, slice thickness 3 mm.

B. Variation of echo time (TE) in fast spin echo

The three orthogonal image plane in part of three actual size of coil packs dimension 2.0x2.0x5.0, 5.6x5.6x9.8 and 6.5x6.5x9.0 mm were obtained from various TE at 8, 10, 15, 60, 80 and 100 ms of pulse sequence fast spin echo. The signal losses due to coil induced or susceptibility artifact values by drawing were determined by ROI. The table of measurement diameter is shown in Table 4.5 to 4.7 respectively.

Table 4.5 Percent error of artifact diameter versus echo time (ms) for fast spin echo, of signal loss due to coil-induced susceptibility artifact

Echo Time(TE, ms)	Axial	Coronal	Sagittal
8	18	125	14
10	18	125	20
15	18	150	24
60	24	160	24
80	28	175	26
100	34	190	30

From the Table 4.5, the smallest percent error was obtained at lowest echo time of 8 ms in fast spin echo.

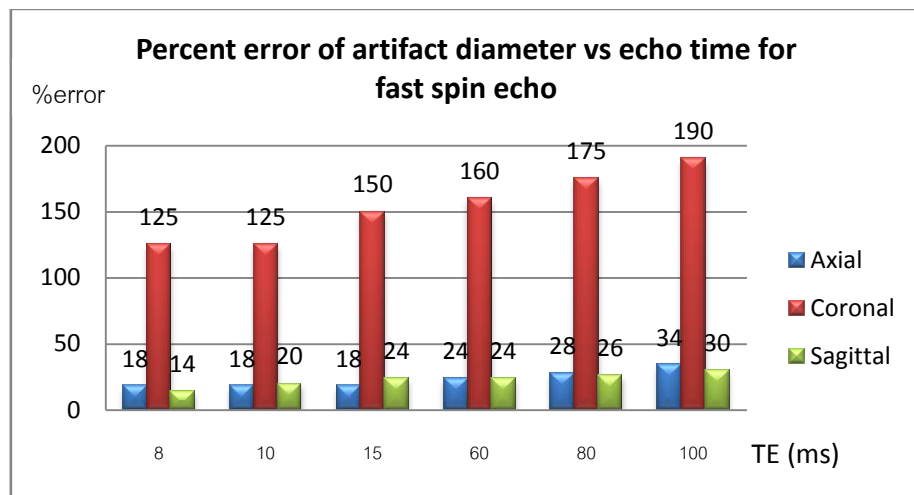


Figure 4.1 The percent error of artifact diameter for fast spin echo versus echo time (ms) in three orthogonal planes from 2.0x2.0x5.0 mm.

Figure 4.1 shows the percent error at an MRI image of fast spin echo images from three orthogonal planes. Actual size diameter is 2.0x2.0x5.0 mm. The percent error at MRI images is shown in the Table 4.5.

Table 4.6 Percent error of artifact diameter versus echo time (ms) for fast spin echo, of signal loss due to coil-induced susceptibility artifact

Fast Spin Echo			
TE (ms)	Axial	Coronal	Sagittal
8	42	53	-10
10	42	60	1
15	46	64	2
60	50	71	2
80	51	75	4
100	57	78	5

From the Table 4.6, the smallest percent error was obtained at lowest echo time of 8 ms in fast spin echo.

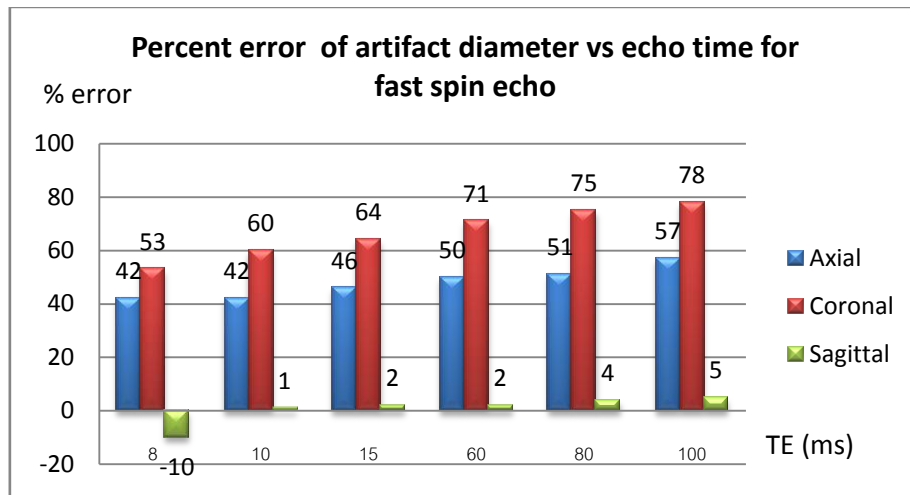


Figure 4.2 The percent error of artifact diameter versus echo time for fast spin echo in three orthogonal planes of 5.6x5.6x9.8 mm.

Figure 4.2 shows the percent error at an MRI image of fast spin echo images from three orthogonal planes. Actual size diameter is 5.6x5.6x9.8 mm. The percent error at MRI images is shown in the Table 4.6.

Table 4.7 Percent error of artifact diameter versus echo time (ms) for fast spin echo, of signal loss due to coil-induced susceptibility artifact

Fast spin echo			
TE (ms)	Axial	Coronal	Sagittal
8	130	29	66
10	146	53	73
15	147	53	77
60	153	56	80
80	156	56	85
100	161	61	87

From the Table 4.7, the smallest percent error was obtained at lowest echo time of 8 ms in fast spin echo.

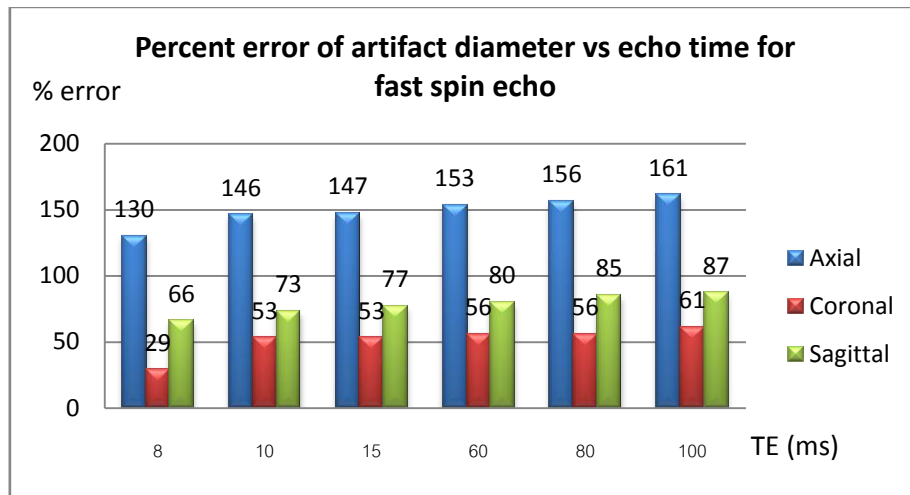


Figure 4.3 The percent error of artifact diameter versus echo time for fast spin echo in three orthogonal planes of 6.5x6.5x9.0 mm.

Figure 4.3 shows the percent error at an MRI image of fast spin echo images from three orthogonal planes. Actual size diameter is 6.5x6.5x9.0 mm. The percent error at MRI images is shown in the Table 4.7.

C. Variation of Echo time (TE) in fast gradient echo

The three orthogonal image plane in part of three actual size of coils pack diameter 2.0x2.0x5.0, 5.6x5.6x9.8 and 6.5x6.5x9.0 mm are obtained from the various TE at 3.5, 4.6, 6.9, 9.2, and 11.5 ms of pulse sequence fast gradient echo. The signal losses due to coil induced or susceptibility artifact values by drawing were determined by ROI. The table of measurement diameter is shown in Table 4.8 to 4.10 respectively.

Table 4.8 Percent error of artifact diameter versus echo time (ms) for fast gradient echo, of signal loss due to coil-induced susceptibility artifact

Echo Time(TE)	Axial	Coronal	Sagittal
3.5	44	190	32
4.6	50	210	36
6.9	72	245	38
9.2	68	280	50
11.5	76	300	56

From Table 4.8 the smallest percent error was obtained at lowest echo time of 3.5 ms in fast gradient echo.

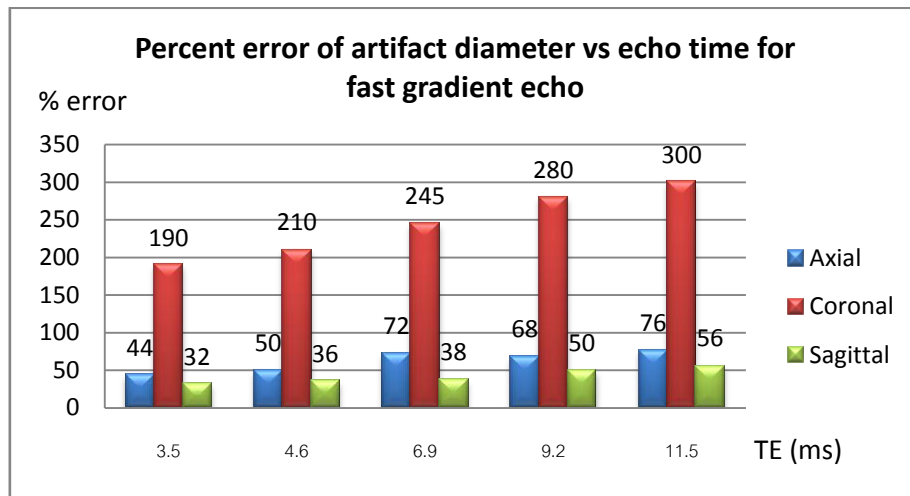


Figure 4.4 The percent error of artifact diameter versus echo time for fast gradient echo in three orthogonal planes of 2.0x2.0x5.0 mm.

Figure 4.4 shows the percent error at an MRI image of fast gradient echo images from three orthogonal planes. Actual size diameter is 2.0x2.0x5.0 mm. The percent error at MRI images is shown in the Table 4.8.

Table 4.9 Percent error of artifact diameter versus echo time (ms) for fast gradient echo, of signal loss due to coil-induced susceptibility artifact

Echo Time(TE)	Axial	Coronal	Sagittal
3.5	9.8	11.8	11.4
4.6	12.1	14.2	12
6.9	12.4	14.6	13.2
9.2	12.7	15.6	15.4
11.5	13.6	16.9	16.8

From the Table 4.9 the smallest percent error was obtained at lowest echo time of 3.5 ms in fast gradient echo.

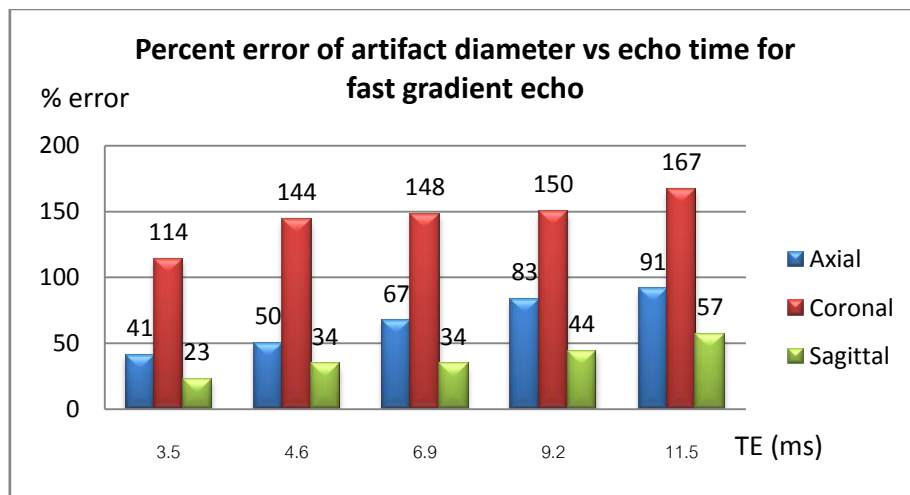


Figure 4.5 The percent error of artifact diameter versus echo time for fast gradient echo in three orthogonal planes of 5.6x5.6x9.8 mm.

Figure 4.5 shows the percent error at an MRI image of fast gradient echo images from three orthogonal planes. Actual size diameter is 5.6x5.6x9.8 mm. The percent error at MRI images is shown in the Table 4.9.

Table 4.10 Percent error of artifact diameter versus echo time (ms) for fast gradient echo, of signal loss due to coil-induced susceptibility artifact

Echo Time(TE)	Axial	Coronal	Sagittal
3.5	167	92	83
4.6	207	106	111
6.9	227	130	133
9.2	250	135	133
11.5	269	161	140

From the Table 4.10, the smallest percent error was obtained at lowest echo time of 3.5 ms in fast gradient echo.

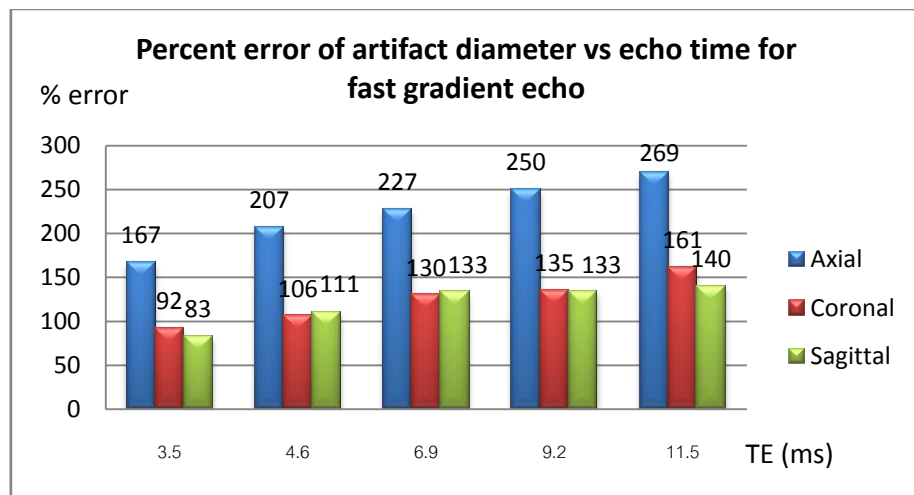


Figure 4.6 The percent error of artifact diameter versus echo time for fast gradient echo in three orthogonal planes of 6.5x6.5x9.0 mm.

Figure 4.6 shows the percent error at an MRI image of fast gradient echo images from three orthogonal planes. Actual size diameter is 6.5x6.5x9.0 mm. The percent error at MRI images is shown in the Table 4.10.

D. Variation of turbo factor in fast spin echo

The three orthogonal image plane in part of three actual size of coils pack diameter 2.0x2.0x5.0, 5.6x5.6x9.8 and 6.5x6.5x9.0 mm are obtained from various Turbo factors at 3, 6, 8,10,16,20 and 24 echo of pulse sequence fast spin echo. The signal losses due to coil induced or susceptibility artifact values by drawing were determined by ROI. The table of measurement diameter is shown in Table 4.10 to 4.1 respectively.

Table 4.11 Percent error of artifact diameter versus turbo factor for fast spin echo, of signal loss due to coil-induced susceptibility artifact

Turbo factor	Axial	Coronal	Sagittal
3	14	65	20
4	18	70	22
5	24	80	28
6	24	80	30
8	26	80	30
10	26	100	30
16	30	100	32
20	36	115	32
24	36	125	36

From Table 4.11 the smallest percent error was obtained at lowest turbo factor of 3 in fast spin echo.

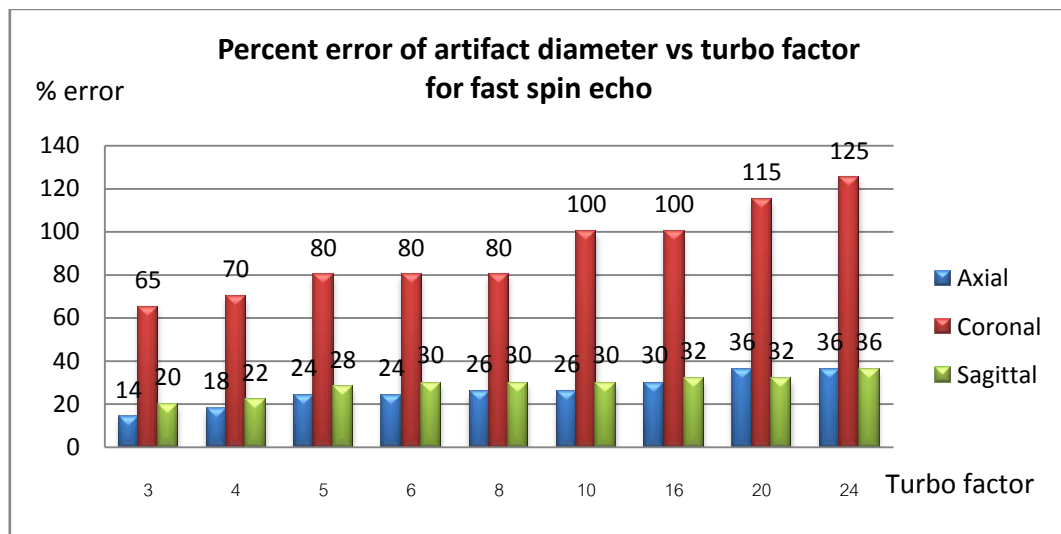


Figure 4.7 The percent error of artifact diameter versus turbo factor for fast spin echo in three orthogonal planes of 2.0x2.0x5.0 mm.

Figure 4.7 shows the percent error at an MRI image of fast spin echo images from three orthogonal planes. Actual size diameter is 2.0x2.0x5.0 mm. The percent error at MRI images is shown in the Table 4.11.

Table 4.12 factor for fast Percent error of artifact diameter versus turbo spin echo, of signal loss due to coil-induced susceptibility artifact

Turbo factor	Axial	Coronal	Sagittal
3	29	78	2
4	60	89	4
5	64	89	10
6	64	89	12
8	71	89	16
10	71	96	16
16	75	96	16
20	78	100	17
24	83	103	20

From Table 4.12 the smallest percent error was obtained at lowest turbo factor of 3 in fast spin echo.

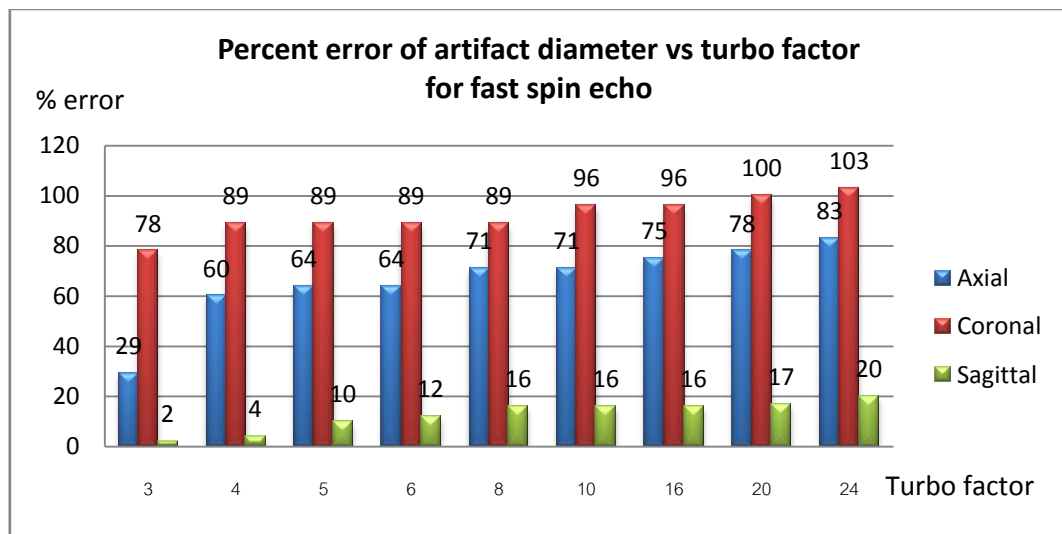


Figure 4.8 The percent error of artifact diameter versus turbo factor for fast spin echo in three orthogonal planes of 5.6x5.6x9.8 mm.

Figure 4.8 shows the percent error at an MRI image of fast spin echo images from three orthogonal planes. Actual size diameter is 5.6x5.6x9.8 mm. The percent error at MRI images is shown in the Table 4.12.

Table 4.13 Percent error of artifact diameter versus turbo factor for fast spin echo, of signal loss due to coil-induced susceptibility artifact

Turbo factor	Axial	Coronal	Sagittal
3	146	35	53
4	146	53	66
5	152	61	72
6	152	61	72
8	155	63	72
10	155	63	77
16	167	64	80
20	167	69	80
24	170	72	82

From the Table 4.13 the smallest percent error was obtained at lowest turbo factor of 3 in fast spin echo.

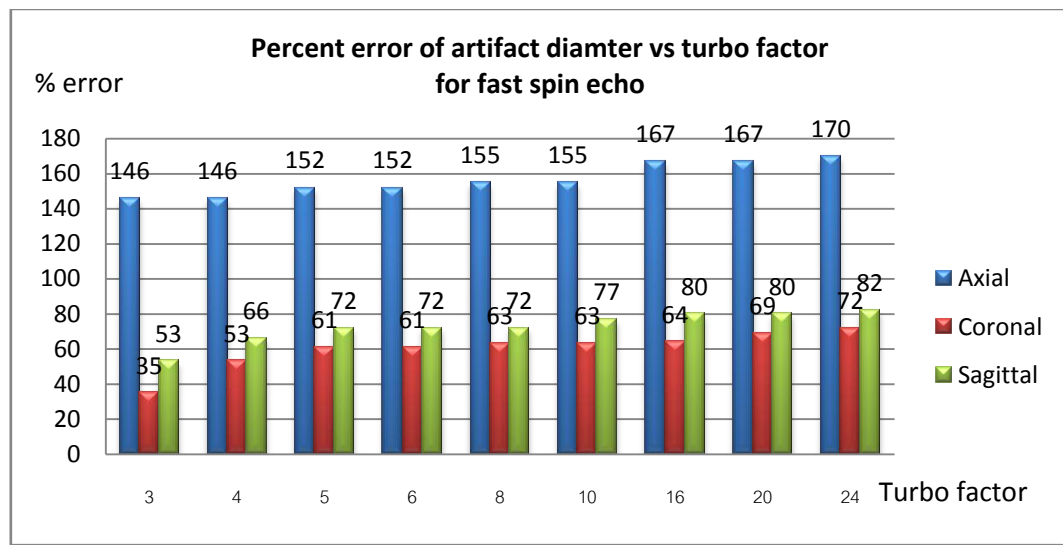


Figure 4.9 The percent error of artifact diameter versus turbo factor for fast spin echo in three orthogonal planes of 6.5x6.5x9.0 mm.

Figure 4.9 shows the percent error at an MRI image of fast spin echo images from three orthogonal planes. Actual size diameter is 6.5x6.5x9.0 mm. The percent error at MRI images is shown in the Table 4.14.

4.3 Volume Measurement Data

The volume and artifact overestimation factor were calculated on the basis of the measured artifact volume compared with actual coil pack volume measurements. The artifact overestimation factors were calculated in the following manner.

$$\alpha_v = v(\text{MRI})/v(\text{coil pack})$$

4.3.1 Evaluation of the artifact volume.

A. Variation of pulse sequence

The three orthogonal planes of actual size of coils packs volume were 26, 160, and 229 mm³ For four pulse sequence MRI 2D images are displayed with the study of the signal loss due to coil induced susceptibility artifact affected by the matrix size of 256x192, 256x256, 512x256 and slice thickness of 3, 5, 7 mm at MRI 3.0 T. The pulse sequence is Spin echo, Fast spin echo, Inversion recovery and Fast gradient echo. The signal loss due to coil induced or susceptibility artifact values by sum of multiple ROI with signal loss rim auto detected. The figure of volume measurement and the table of volume overestimation factor are shown as in Figure 4.10-4.12 and Table 4.13-4.15.

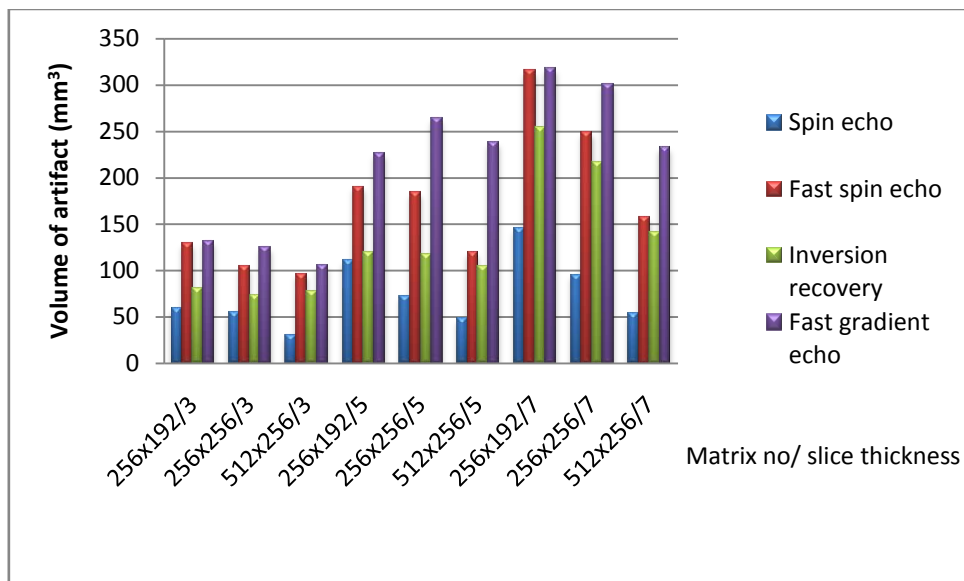


Figure 4.10 The signal loss volumes (mm^3) versus pulse sequence at different, matrix size and slice thickness of volume of coil pack 26 mm^3 .

Figure 4.10 shows signal loss volumes (mm^3) obtained at pulse sequence fast gradient echo produced largest artifact than spin echo, fast spin echo and inversion recovery. The spin echo sequence, the smallest signal loss volume is obtained.

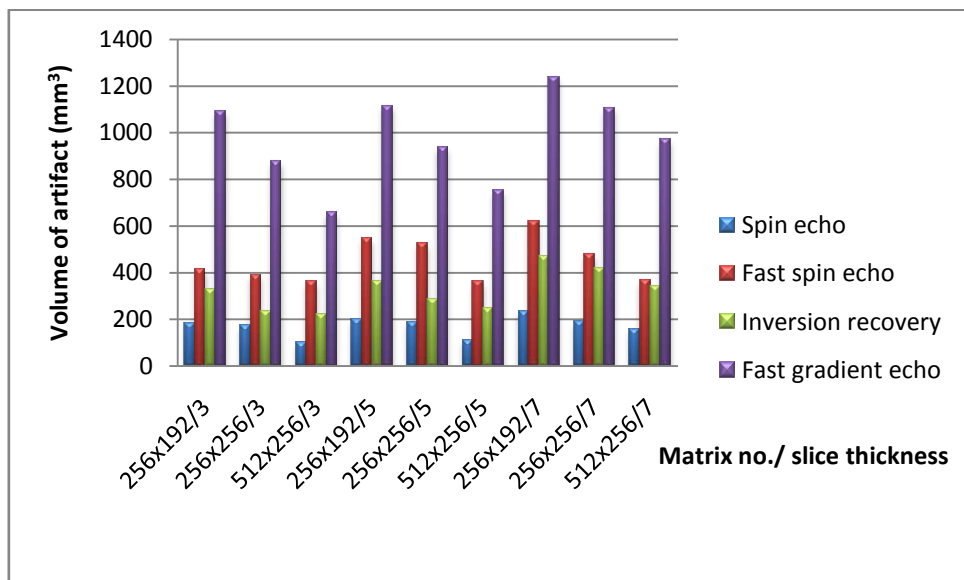


Figure 4.11 The signal loss volumes (mm^3) versus pulse sequence, matrix size and slice thickness of volume of coil pack 160 mm^3 .

Figure 4.11 show largest signal loss volumes (mm^3) obtained at fast gradient echo sequence produced artifact than Inversion recovery, Spin echo and fast spin echo sequence. The fast spin echo sequence, the smallest signal loss volume is obtained.

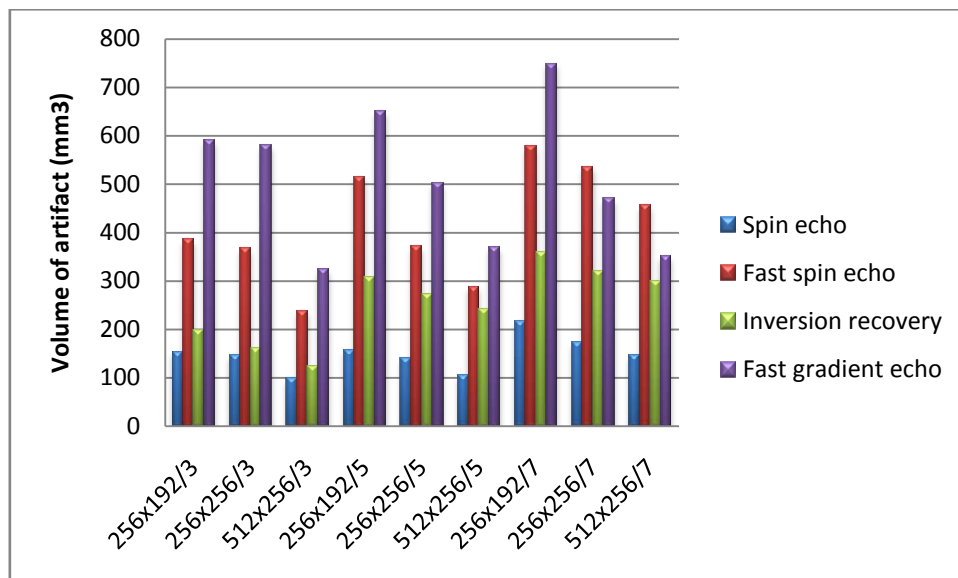


Figure 4.12 The signal loss volumes (mm^3) versus pulse sequence at different, matrix size and slice thickness of volume of coil pack 229 mm^3 .

Figure 4.12 shows signal loss volumes (mm^3) obtained at fast gradient echo sequence produced largest artifact than Inversion recovery, Fast spin echo and Spin echo sequence. The fast spin echo sequence, the smallest signal loss volume is obtained.

B. Volume overestimation factor for given sequence

The three orthogonal planes an actual size of coils packs volume were 26, 160, and 229 mm^3 . For four pulse sequence MRI images are displayed with the study of the signal loss due to coil induced susceptibility artifact affected by the matrix size of 256x192, 256x256, 512x256 and slice thickness of 3, 5, 7 mm at MRI 3.0 T. The pulse sequence is Spin echo, Fast spin echo, Inversion recovery and fast gradient echo. The volume overestimation factor of susceptibility artifact calculated by formula $\alpha_v = v(\text{MRI})/v(\text{coil pack})$. The table of volume overestimation factor is shown as in Table 4.14-4.16.

Table 4.14 Volume overestimation factor (mm^3); in pulse sequence due to coil-induced susceptibility artifact actual size of coil volume (26 mm^3).

Matrix size/Slice thickness	Spin Echo	Fast Spin Echo	Inversion Recovery	Fast Gradient Echo
256x192/3	9.8	8.6	5.33	8.73
256x256/3	8.46	6.9	4.86	8.33
512x256/3	4.0	6.4	5.13	7.0
256x192/5	9.2	12.66	7.93	15.06
256x256/5	9.2	12.26	7.8	17.6
512x256/5	7.8	7.93	6.93	15.86
256x192/7	17.33	21.0	16.93	21.2
256x256/7	19.13	16.6	14.46	20.06
512x256/7	15	10.46	9.4	15.46

From the Table 4.14, the highest volume overestimation factor (mm^3) was obtained at fast gradient echo. The spin echo pulse sequence, the smallest overestimation factor is obtained.

Table 4.15 Volume overestimation factor (mm^3); in pulse sequence due to coil-induced susceptibility artifact actual size of coil volume (160 mm^3).

Matrix size/Slice thickness	Spin Echo	Fast Spin Echo	Inversion Recovery	Fast Gradient Echo
256x192/3	3.03	2.54	2.35	6.03
256x256/3	2.63	2.48	2.21	5.37
512x256/3	2.12	1.9	1.93	5.22
256x192/5	3.93	3.71	2.66	6.96
256x256/5	3.03	3.52	2.48	6.53
512x256/5	2.41	3.24	2.41	6.11
256x192/7	4.89	5.63	4.1	7.68
256x256/7	4.83	5.39	3.85	7.34
512x256/7	3.43	5.01	3.51	6.75

From the Table 4.15, the highest volume overestimation factor (mm^3) was obtained at fast gradient echo; the fast spin echo pulse sequence, the smallest overestimation factor is obtained.

Table 4.16 Volume overestimation factor (mm^3); in pulse sequence due to coil-induced susceptibility artifact as actual size of coil volume (229 mm^3).

Matrix size/Slice thickness	Spin Echo	Fast Spin Echo	Inversion Recovery	Fast Gradient Echo
256x192/3	3.77	2.77	1.94	5.11
256x256/3	3.67	2.64	1.72	4.55
512x256/3	2.93	1.67	1.67	4.15
256x192/5	5.46	3.89	4.06	5.71
256x256/5	4.86	3.88	3.45	5.07
512x256/5	4.13	2.88	3.23	4.89
256x192/7	6.76	4.99	4.73	7.6
256x256/7	4.85	4.77	4.41	5.78
512x256/7	4.38	4.62	4.08	4.53

From Table 4.16, the largest volume overestimation factor (mm^3) was obtained at fast gradient echo. The fast spin echo pulse sequence, the smallest overestimation factor is obtained.

4.4 Quantitative assessment

The signal intensity loss volume data and the overestimation data were analyzed with an Analysis of Variance (ANOVA). The diameter data in the three planes (Axial, Coronal, Sagittal) were also analyzed with ANOVA test. The effect of parameter changes, coil packs and different sequence were analyzed. The null hypothesis was rejected at $P \leq 0.05$. The analysis of variance were calculated in terms of significantly as shown in Table 4.16 to 4.19.

Table 4.17 The data for quantitative assessment of signal intensity loss as three planes diameter. The actual size of coil volume 26 mm^3

Sequence		Sum of Squares	df	Mean Square	F	Sig
FGRE	Between Groups	183	2	0.091	0.163	0.001
	Within Group	13.493	24	0.562		
	Total	13.676	26			
FSE	Between Groups	4.776	2	2.388	25.307	0.001
	Within Group	2.264	24	0.094		
	Total	7.040	26			
IR	Between Groups	5.970	2	2.985	10.409	0.001
	Within Group	6.882	24	0.287		
	Total	12.852	26			
Spin echo	Between Groups	16.121	2	8.060	28.654	0.001
	Within Group	6.751	24	0.281		
	Total	22.872	26			

FGRE = fast gradient echo, **FSE** = fast spin echo, **IR** = inversion recovery

From Table 4.17. The quantitative assessment by analysis of variance of signal intensity loss diameter values were representing the significant as fast spin echo (FSE), inversion recovery (IR) and Spin echo (SE) group. The null hypothesis was rejected at $P \leq 0.05$.

Table 4.18 The data for quantitative assessment of signal intensity loss as three planes diameter. The actual size of coil volume 160 mm^3

Sequence		Sum of Squares	df	Mean Square	F	Sig
FGRE	Between Groups	143.736	2	71.868	92.008	0.001
	Within Group	18.747	24	0.781		
	Total	162.483	26			
FSE	Between Groups	0.287	2	0.144	0.079	0.001
	Within Group	43.640	24	1.818		
	Total	43.927	26			
IR	Between Groups	7.347	2	3.674	5.050	0.015
	Within Group	17.460	24	0.728		
	Total	24.807	26			
Spin echo	Between Groups	20.062	2	10.031	11.999	0.001
	Within Group	20.064	24	0.836		
	Total	40.127	26			

FGRE = fast gradient echo, **FSE** = fast spin echo, **IR** = inversion recovery

From Table 4.18 The quantitative assessment by analysis of variance of signal intensity loss diameter values were representing the significant as fast gradient echo (FGRE), inversion recovery (IR) and Spin echo (SE) group. The null hypothesis was rejected at $P \leq 0.05$.

Table 4.19 The data for quantitative assessment of signal intensity loss as three planes diameter. The actual size of coil volume 229 mm^3

Sequence		Sum of Squares	df	Mean Square	F	Sig
FGRE	Between Groups	66.380	2	33.190	30.995	.001
	Within Group	25.700	24	1.071		
	Total	92.080	26			
FSE	Between Groups	89.014	2	44.507	109.869	.001
	Within Group	9.722	24	.405		
	Total	98.736	26			
IR	Between Groups	33.290	2	16.645	24.504	.001
	Within Group	16.302	24	.679		
	Total	49.592	26			
Spin echo	Between Groups	194.481	2	97.240	103.213	.001
	Within Group	22.611	24	.942		
	Total	217.092	26			

FGRE = fast gradient echo, **FSE** = fast spin echo, **IR** = inversion recovery

From Table 4.19 The quantitative assessment by analysis of variance of signal intensity loss diameter values were representing the significant as any sequence. The null hypothesis was rejected at $P \leq 0.05$.

Table 4.20 The data for quantitative assessment of signal intensity loss as three volume size of coil packs. The actual size of coil volume 229 mm^3

Sequence		Sum of Squares	df	Mean Square	F	Sig
FGRE	Between Groups	2773262.000	2	1386631.000	55.506	0.001
	Within Group	599560.667	24	24981.694		
	Total	3372822.667	26			
FSE	Between Groups	416655.630	2	208327.851	22.767	0.001
	Within Group	219607.778	24	9150.324		
	Total	636263.407	26			
IR	Between Groups	170339.852	2	85169.926	15.373	0.015
	Within Group	132966.222	24	5540.259		
	Total	303306.074	26			
Spin echo	Between Groups	45854.889	2	22927.444	15.920	0.001
	Within Group	34563.111	24	1440.130		
	Total	80418.000	26			

FGRE = fast gradient echo, **FSE** = fast spin echo, **IR** = inversion recovery

From Table 4.20 The quantitative assessment by analysis of variance of signal intensity loss volumes were representing the significant as any sequence. The null hypothesis was rejected at $P \leq 0.05$.

CHAPTER V

DISCUSSION AND CONCLUSION

5.1 Discussion

MRI is a digital, imaging modality of great flexibility with respect to image contrast and its spatial characteristics. However, one of the downsides of this flexibility is a greater complexity in terms of the choice of scanning parameters. In general, the scan times are not negligible and there is a certain tendency towards artifact. However, it was agreed that the fundamental limitation in MRI is the susceptibility artifact which depends on the hardware, particularly the main field strength (B_0).

Platinum coils are non-ferromagnetic and paramagnetic materials which have the potential to align along the direction of the lines of magnetic flux and display a force proportional to not only the gradient but also to the field strength [19].

In this in vitro study, some of the major characteristic related to MRI imaging of coil packs have been defined. The main conclusions are 1.spin echo (SE) and fast spin echo (FSE) with reduced echo train length reduce the susceptibility artifact; 2.susceptibility artifact increases with increased slice thickness; 3.susceptibility artifact increases with decreased matrix size; 4.reducing the echo time (TE) is the main factor in improving susceptibility artifact on fast gradient sequence; 5.susceptibility artifact increases with increased coil packs density; and asymmetric artifact occurs in the frequency encoding direction on MRI images.

5.1.1 Assessment of susceptibility artifact in Pulse sequence. The technical assessments of susceptibility artifact of the MRI image were studied by the investigation of local signal loss and image distortion. To directly characterize the local signal loss and image distortion, the volume of coil packs with diameter of coil packs were measured as shown in Figure 5.1.

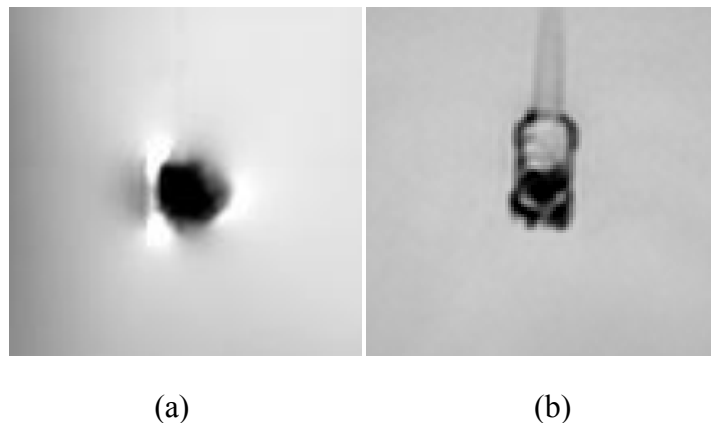
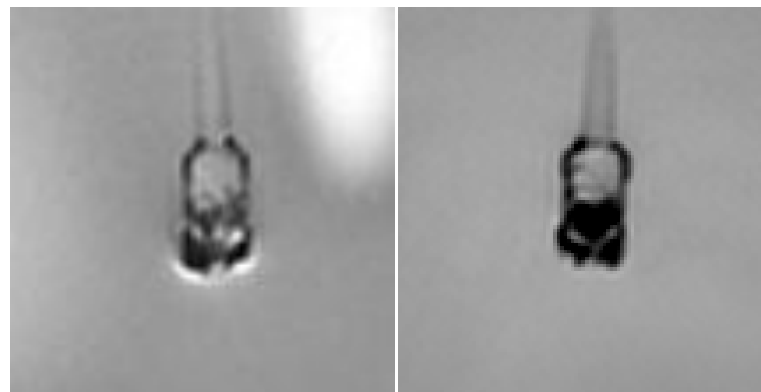


Figure 5.1 The image of susceptibility artifact from Aluminum (a) and neuro endovascular coil (b)

The MR imaging performed with Spin echo and fast spin echo pulse sequence, a 180° refocusing pulse enables recovery of the transverse signal lost because of the inhomogeneity of the static magnetic field and bulk susceptibility differences. Substantial magnetic field inhomogeneity caused by bulk ferromagnetic materials result in additional local dephasing of the spins of hydrogen protons in randomly diffusing water molecules, and this diffusion-related dephasing is not recoverable with the application of a 180° refocusing pulse. This type of dephasing, contributes directly to the overall local signal loss in the vicinity of neuro endovascular coil (Figure 5.2).



(a)

(b)

Figure 5.2 Image of neuro endovascular coil from Spin echo (a) and fast spin echo (b) pulse sequence

The characteristics of the MRI images fast gradient echo (FGRE) pulse sequences include no 180° refocusing pulse. As a consequence, FGRE pulse sequences allow no correction for large and fixed magnetic field inhomogeneity induced by neuro endovascular coil. Such magnetic field inhomogeneity cause marked intravoxel dephasing (T_2^* effect) and result in local signal loss (Figure 5.3). In the routine protocol, Time of Flight (TOF) is fast gradient echo technique used for Contrast Enhance MRA (CE-MRA) and Non Contrast Enhanced MRA. The TE is short (TE 3.5 ms) and susceptibility induced signal intensity loss is minimal. The fast gradient echo sequence produced the least amount of artifact overall and differ significantly from the longer TE sequence.

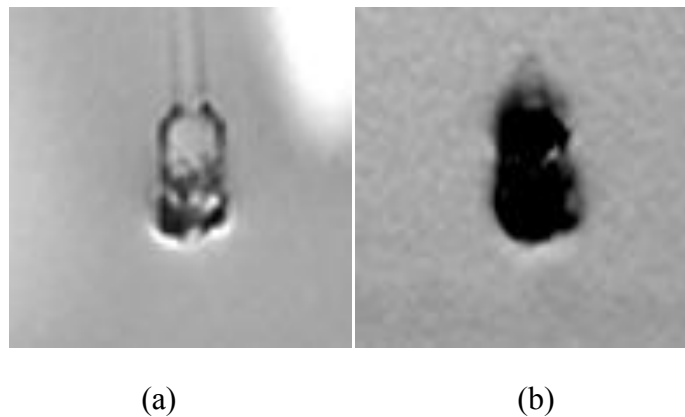


Figure 5.3 The susceptibility artifacts of Spin echo (a) and Fast gradient echo (b).

From figure 5.3 shows susceptibility artifacts between Spin echo (a) and fast gradient echo (b). Spin echo causes smaller artifacts than fast gradient echo.

5.1.2 Assessment of susceptibility artifact in Turbo factor (TSE factor)

The longer turbo factor, the echoes at the end of the echo train are more susceptible to dephasing. High-frequency data responsible for image detail are acquired at the beginning and at the end of the echo train, if conventional linear filling of the k-space is used. Therefore, more blurring (less image sharpness) is expected with longer turbo factor because of progressive dephasing. At 3 T more signals is available but spins dephase more quickly. Furthermore, the use of a short turbo factor is reducing susceptibility artifact of metal (Figure 5.5).

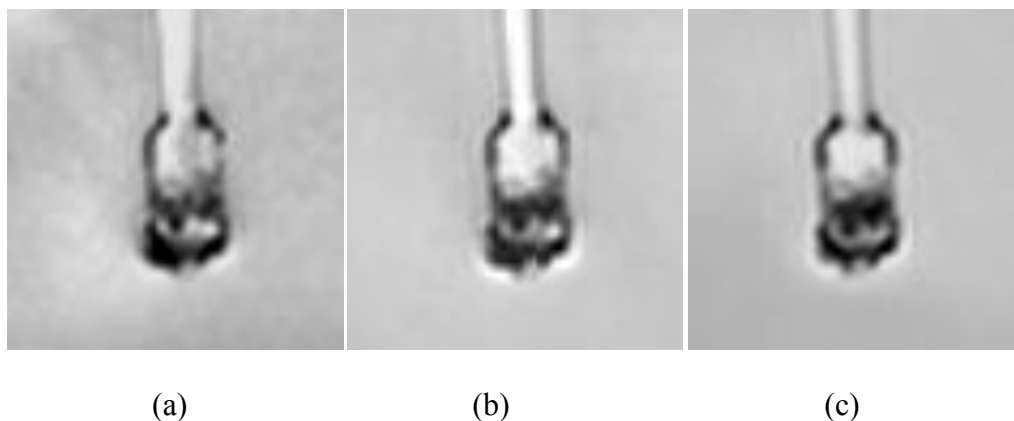


Figure 5.4. Susceptibility artifacts from Turbo factor 3 (a), 8 (b) and 24 (c).

From figure 5.4 imaging at low turbo factor (a) shows smaller artifacts than (b) and (c) respectively.

5.1.3 Assessment of susceptibility artifact in Voxel size

The voxel size is determined by the field of view, image matrix, and section thickness selected at image acquisition. The use of a small voxel size increases the spatial definition of a signal distortion surrounding a metallic device but has little if

any effect on the apparent size of the corresponding artifact. Furthermore, the use of a small voxel size helps reduce diffusion-related signal loss in the vicinity of neuro endovascular coil (Figure 5.5-5.6).

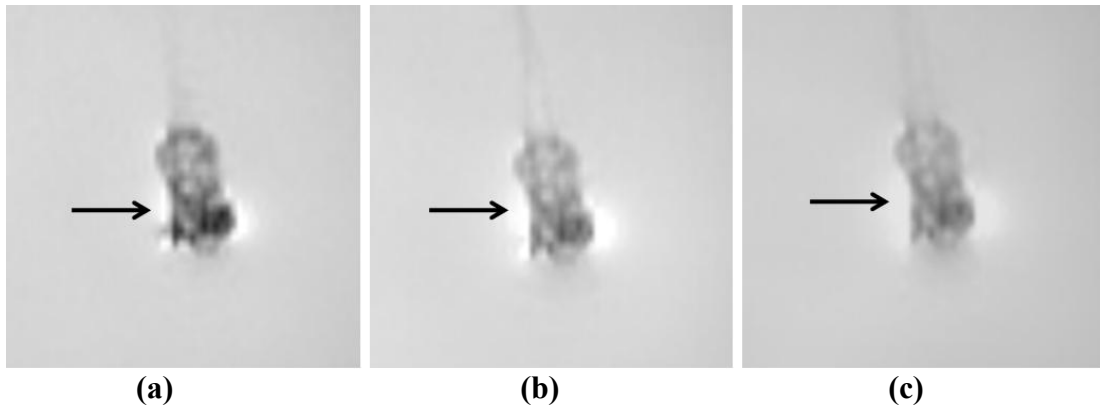


Figure 5.5 Susceptibility artifacts between Slice thickness 3 (a), 5 (b) and 7 mm (c).

From figure 5.5 the thin slice 3mm (a) shows smaller artifacts than thick slice 5 and 7 mm in (b) and (c) respectively. Represent hyper signal at rim of the signal loss artifact in thick slice thickness.

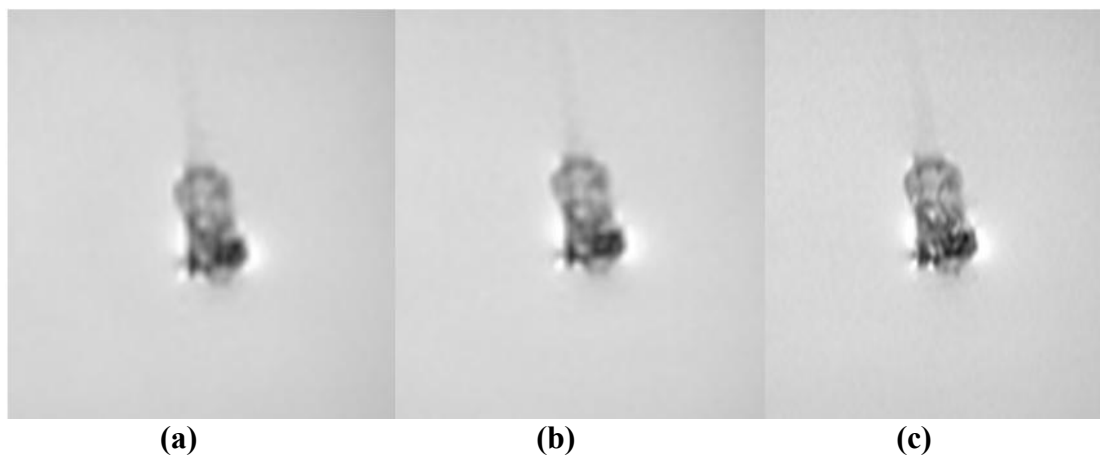


Figure 5.6 Susceptibility artifacts between matrix sizes 256x192 (a), 256x256 (b) and 512x256 (c).

From figure 5.6, the small matrix sizes (a) results in higher artifacts than in larger matrix size in (b) and (c) respectively. Coil aneurysm remnants were better characterized with large matrix sizes.

5.1.4 Assessment of susceptibility artifact in Echo time (TE)

Image degradation from neuro endovascular coil in MRI image is the result of magnetic field heterogeneity and susceptibility induced signal intensity loss. Local distortion of the magnetic field is secondary to differences in the static magnetic susceptibility of the metal and surrounding tissue and the presence of dynamic eddy currents as from radio-frequency pulses and gradient magnetic fields. Reducing the TE has been shown to reduce heterogeneity of the magnetic field that occurs with metal.

In this study: the change in TE resulting in a statistically significant reduction in susceptibility artifact. Reducing the TE from 11.5ms to 3.5 ms in FGRE sequence was effective at minimizing artifact while limiting overall image degradation.

Therefore, reducing the TE can result in improved visualizing of peri-aneurysmal soft tissues and also there is less incremental benefit once the TE is below 3.5 ms as in Figure 5.7-5.8.

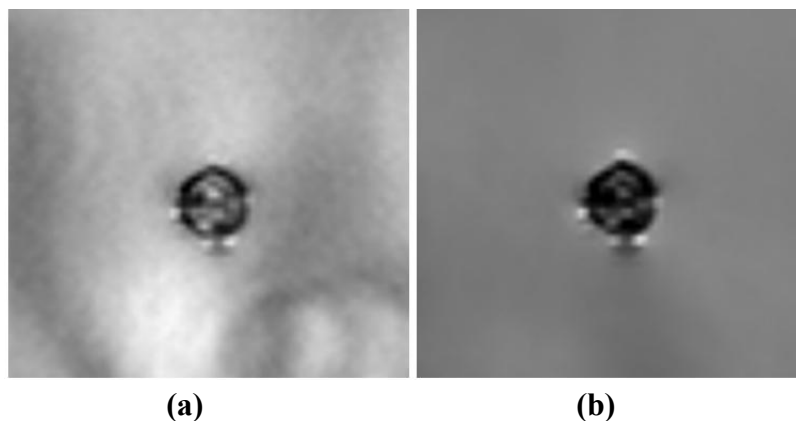


Figure 5.7 Susceptibility artifacts between Fast spin echo sequence Echo time (TE) 8 ms (a) and 24 ms (b).

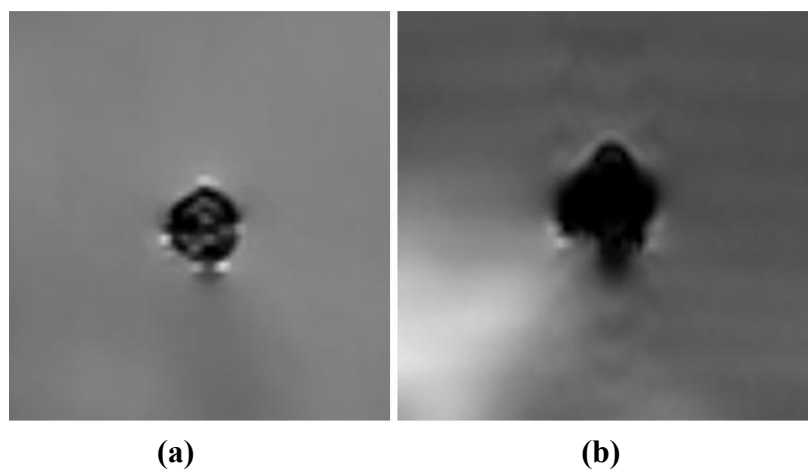


Figure 5.8 Susceptibility artifacts between fast gradient echo sequence Echo time (TE) 3.5 ms (a) and 11.5 ms (b).

Figure 5.7 and 5.8 show the shorter TE (a), with fewer artifacts than (b). Improved visualization of perianeurysmal soft tissues is the best accomplished by reducing the TE on any sequence.

5.1.5 Frequency Encoding Direction

The frequency encoding direction yields the highest artifact across all coil packs. The data were collected in the axial plane such that the frequency encoding gradient was oriented along the anterior to posterior. With this prescription, the frequency gradient was significantly smaller in magnitude than the other two directions. Thus, the relative effect of magnetic susceptibility was greatest in the frequency direction. In typical clinical applications, the frequency encoding gradient for 3D TOF MRA (fast gradient echo sequence) is oriented in the AP direction. These data suggest that the orientation of the frequency encoding direction matters and will asymmetrically degrade image quality in that direction as shown in Figure 5.8 [5.2].

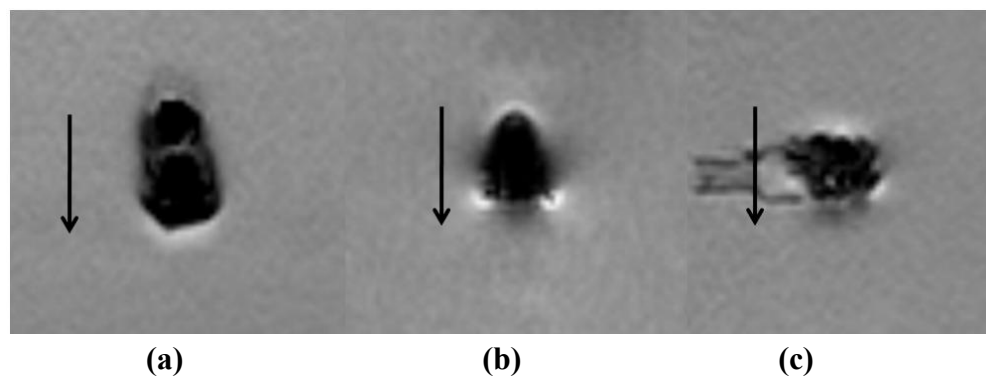


Figure 5.9 The susceptibility artifacts in three orthogonal planes Axial (a), Coronal (b) and Sagittal (c).

From figure 5.9 the shape of the susceptibility artifact along the axis of frequency encoding, the arrow in image shows the direction of the frequency encoding gradient.

5.1.6 Overestimation Factor

Overestimation factors were calculated to compare volume artifact measurements to actual volume measurements. As expected, less overestimation occurred at Spin echo pulse sequence, high matrix size, thin slice and less densely coil packs as shown in Table 5.1.

Table 5.1 Overestimation factors

Matrix size/Slice thickness	Spin Echo	Fast Spin Echo	Inversion Recovery	Fast Gradient Echo
256x192/3	3.03	2.54	2.35	6.03
256x256/3	2.63	2.48	2.21	5.37
512x256/3	2.12	1.9	1.93	5.22
256x192/5	3.93	3.71	2.66	6.96
256x256/5	3.03	3.52	2.48	6.53
512x256/5	2.41	3.24	2.41	6.11
256x192/7	4.89	5.63	4.1	7.68
256x256/7	4.83	5.39	3.85	7.34
512x256/7	3.43	5.01	3.51	6.75

5.1.7 Clinical Relevance

Endovascular coil can be assessed by MRI and MRA for the neuro aneurysm, but there are many factors affecting the imaging strategy. 3D TOF (fast gradient echo sequence) imagings of endovascular coils are more successful at 3 Tesla MRI. Significant reductions in susceptibility artifact induced signal loss can be achieved by reducing the voxel size, for example: black blood image is the high resolution proton density image and TE to the 3.5 ms range for example, and non contrast enhanced MRA. Aneurysm of lower coil packs density that are considered partially or incompletely treated will be more easily studied particular at 3.0 T but should be adjust parameters for the decreased artifact production. A heterogeneous coil pack may favorably affect visualization if the dome, for instance, is more densely coiled than the neck, which is often the case.

The benefits of 3 Tesla imaging, include improved signal to noise ratio (SNR), spatial resolution, and temporal resolution, but increase susceptibility artifact which induced signal intensity loss and provide an opportunity for Contrast enhanced MRA (CE-MRA) as the fast gradient echo applications in patients with coiled aneurysms.

5.1.8 Sequence development

In the future sequence development, View angle tilting (VAT) uses an extra gradient in the slice select direction during the read-out gradient, and the slice is effectively viewed from an angle. The sum of artefactual frequency shifts in the slice select and the frequency encoding direction results in a frequency shift with oblique direction. By viewing from this oblique angle during read-out, the received signals can be projected into the correct pixel of the image matrix. Although in-plane spatial distortion is considerably reduced, blur is introduced into the MR image. Recently, it has been shown that this blurring may be avoided using a technique with multiple VAT read-outs. Several small series have been published to demonstrate the clinical use of VAT in musculoskeletal MR imaging including the spine. The MARS (metal artifact reduction sequence) technique is a sequence combining VAT with increased slice select gradient and increased read-out bandwidth [20].

5.2 Study Limitations

There are several limitations to this study, including a static phantom, hand measurement, heterogeneity of the coil packs or artifact, and the timing of imaging. Aneurysm model was a closed system with no flow: no estimation on the effects of flowing blood, particularly within the aneurysm, can be made. Also, without flow information, the effect of reducing the TE on the overall quality of the MRI and MRA image cannot be determined. The aneurysm models were hand measured, which can introduce error. Furthermore, the volume measurements were obtained by hand measuring each section only once. No assurance can be given regarding coil pack homogeneity, although clinically, coil packing is typically heterogeneous. Artifact from metal is heterogeneous and represented as signal intensity loss and signal intensity hyper intense. The results described were obtained by using specific image sequence as implemented on Philips Achieva equipment. Different results might be obtained with other equipment or vendors because of different gradient amplitude combinations employed in the sequence structure; however, the conclusions should remain the same.

5.3 Conclusions

Improved visualization of aneurysm and perianeurysmal soft tissues are best accomplished by spin echo sequences and are significantly preferred than Fast spin echo ($P \leq 0.05$), Inversion recovery and Gradient echo sequences because the former apply a 180° refocusing pulse in the middle (at half the echo time) between the 90° radiofrequency (RF) excitation pulse and the read-out of signals at time TE (echo time). Dephasing of spins caused by susceptibility gradients is compensated for by this 180° refocusing pulse, and the loss of signal by dephasing decreased.

Fast spin echo or turbo spin echo sequences are even better suited to reduce metal artifact because multiple 180° refocusing pulses are applied (one for each echo). Furthermore, shorter turbo factor and shorter effective TE in the latter sequences are beneficial for the same reason as sequences having shorter TE. Sequences with a shorter TE are preferred because there is less time for dephasing and frequency shifting between the 90° RF pulse and the signal read-out.

Frequency encoding direction may be useful for adjust is the specific anatomic area involved by the susceptibility artifact. The arrow-shaped susceptibility artifact typically points in the frequency encoding direction and covers more of the anatomy in this direction. Switching the phase and frequency encoding direction changes the direction of the arrow-shaped artifact, but not the size of the artifact.

The slice select gradient is achieved by choosing a smaller slice thickness, and that through-plane susceptibility artifact decreased. In-plane susceptibility artifact decreased by increasing the readout image matrix. The disadvantage of all these measures using stronger gradients is a decrease in signal-to-noise ratio (SNR).

Aneurysms with higher coil pack density produce more artifacts under all conditions. More artifacts are produced in the frequency encoding direction than in other direction [11].

References

- [1] Liney, P.L. Magnetic Resonance Imaging (MRI).The University of Hull. [Online].2005
Available from: www.hull.ac.uk/mri/lectures/gpl_page.html
- [2] Donald, W.M., Moor, E.A., Graves, M.J., and Prince, M.R. MRI from picture to proton. Cambridge: The United Kingdom at the University Press (2004).
- [3] Puddephat's, M. Principle of magnetic resonance imaging. London: Riverside internet 2011:
<http://www.mikepuddephat.com>.
- [4] Brown, M.A., and Semelka, R.C. MR Imagine Abbreviation, Definitions, and Descriptions: A Review. Radiology 213(1999): 647-662.
- [5] Coyne, K. MRI: A Guide Tour. National High magnetic Field Laboratory 2011:
<http://www.magnet.fsu.edu>
- [6] Hoa, D. Image quality and artifacts. Montpellier Cedex 2: IMAIOS SAS, 2008:
<http://www.imaios.com>
- [7] Gallagher, A.T., Nemeth, A.J., and Hacein-Bey, L. An Introduction To the Fourier Transform: Relationship to MRI.AJR 190(2008): 1396-1405
- [8] Lee, V.S., et al. Body and Cardiovascular MR Imaging at 3.0 T. Radiology 244(2007):629-705.
- [9] Molyneux, A., et al. International Subarachnoid Aneurysm Trial (ISAT) of neurosurgical clipping versus endovascular coiling in 2,143 patients with ruptured intracranial aneurysms: a randomised trial. Lancet 360(2002): 1267-74.
- [10] Hennemeyer, C. T., Wicklow, K., Feinberg, D. A., and Derdeyn, C.P. In Vitro Evaluation of Platinum Guglielmi Detachable Coils at 3 T with a Porcine Model: Safety Issues and Artifacts. Radiology 219 (2001): 732–737.
- [11] Walker, T.,et al. MR Angiographic Evaluation of Platinum Coil packs at 1.5T and 3T:An in vitro assessment of Artifact Production. AJNR Am J Neuroradiol. 26(2005):848-853.

- [12] Lee, M.J., Kim, S., and Lee, S.A. Overcoming Artifacts from Metallic Orthopedic Implants at High-Field-Strength MR Imaging and Multidetector CT. RadioGraphics 27 (2007):791–803.
- [13] Frank , S.G. Metallic neurosurgical implants: evaluation of magnetic field interactions, heating, and artifacts at 1.5-Tesla. Magn Reson Imaging 14(2001): 295-9.
- [14] Farrelly, C., Davarpanah, A., Brennan, S.,Sompson, M., and Eustace, S.J. Imaging of Soft Tissues Adjacent to Orthopedic Hardware: Comparison of 3-T and 1.5-T MRI.AJR 194(2010): 60-64.
- [15] Kakeda, S., et al. MRA of intracranial aneurysms embolized with platinum coils: a vascular phantom study at 1.5T and 3T.Magn Reson Imaging 28(2008): 13-20.
- [16] GE Coperate. AW Volumeshare. GE Healthcare 2011: www.gehealthcare.com/international/aw/index.html
- [17] American College of Radiology. Magnetic Resonance Imaging (MRI) Quality Control Manual. Reston. VA (2008).
- [18] American Association of Physicists in Medicine. Acceptance Testing and Quality Assurance Procedures for Magnetic Resonance Imaging Facilities. College Park, MD (2010).
- [19] Kanal, E., and Shellock ,F.G.The value of published data on MR compatibility of metallic implants and devices. AJNR Am J Neuroradiol 15(1993): 1394-1396.
- [20] Vandevenne, J.E., et al. Reduction of Metal Artefact in Musculoskeletal MR I imaging. JBR–BTR 90(2007): 345-349.

Appendices

Appendix A: Case record form

Signal loss volumes (mm³)

Pulse Sequence			
Actual coil volume	15 mm ³	241 mm ³	298 mm ³
Matrix size And Slice thickness	Measured susceptibility artifact volume (mm ³)		
256x192/3 mm			
256x256/3 mm			
512x256/3 mm			
256x192/5 mm			
256x256/5 mm			
512x256/5 mm			
256x192/7 mm			
256x256/7 mm			
512x256/7 mm			

Diameter (mm) in 3 orthogonal planes of signal loss

Pulse Sequence			
Matrix size And Slice thickness	Measured susceptibility artifact diameter (mm)		
Actual coil diameter	5x2x5 mm(A/C/S)	5.6x5.6x9.0 mm(A/C/S)	7.6x6.5x9.0 mm(A/C/S)
256x192/3 mm			
256x256/3 mm			
512x256/3 mm			
256x192/5 mm			
256x256/5 mm			
512x256/5 mm			
256x192/7 mm			
256x256/7 mm			
512x256/7 mm			

A, Axial; C, Coronal; S, Sagittal

Volume overestimation factor for given coil packs density

Pulse Sequence			
Matrix size And Slice thickness	Volume overestimation factor		
Actual size coil	15 mm ³	241 mm ³	298 mm ³
256x192/3 mm			
256x256/3 mm			
512x256/3 mm			
256x192/5 mm			
256x256/5 mm			
512x256/5 mm			
256x192/7 mm			
256x256/7 mm			
512x256/7 mm			

Volume overestimation factor = Volume of artifact/ Volume of coil pack

Diameter (mm) in 3 orthogonal plane of signal loss

Turbo Spin Echo			
Actual coil diameter	(mm)		
Turbo Factor	Axial	Coronal	Sagittal
3			
8			
12			
16			
24			

Turbo Spin Echo			
Actual coil diameter	(mm)		
TE (ms)	Axial	Coronal	Sagittal
2			
8			
20			
30			

Appendix B: Quality control of MRI systems

Site: Ramathibodi Hospital **Date:** 16/06/2011

Serial Number: 10148

Equipment:

MRI System Manufacturer: Philips Medical System

Model: Achieva 3.0 Tesla

Processor Manufacturer: Intel(R)

Model: Xenon™.....64 bit.....

QC Phantom: ACR Phantom

Serial number: J10477

Made in U.S.A

Determination of seven aspects of image quality

- Geometric accuracy
- High-contrast spatial resolution
- Slice thickness accuracy
- Slice position accuracy
- Image intensity uniformity
- Percent-signal ghosting
- Low-contrast object detectability

Procedures the QC Phantom

Place the QC phantom on the phantom holder with head coil, and level it. Turn the knob facing the cradle to tilt the top of the phantom away from the gantry. Use the laser alignment lights to position the phantom:

The MRI accreditation program requires the acquisition of a sagittal localizer and four axial series of images. The same set of eleven slice locations within the phantom is acquired in each of the four axial series. These images are acquired using the scanner's head coil. The scan parameters for the localizer and the first two axial series of images are fully prescribed by the ACR in the scanning instructions as the

ACR sequence or ACR images. The third and fourth series of axial images are based on Ramathibodi Hospital is the Spin echo T1 and T2 protocols and are referred to as the set sequences or site images. To discuss the image data it is convenient to introduce names for the different sets of image and numbering for the slice locations within the phantom.

The localizer is a 20 mm thick single slice spin echo acquisition through the center of the phantom, and is referred to simply as the **localizer**.

The first axial series is a spin echo acquisition with ACR specified scan parameters that are typical of T1-weighted acquisitions. This series is called the ACR T1 series.

The second axial series is a double spin echo acquisition with ACR specified scan parameters that are typical of proton density/T2-weighted acquisitions. When analyzing data from this acquisition only the second-echo image are used. The set of second-echo image from this acquisition is called the ACR T2 series.

The third and fourth axial series re based on the scan parameter at Ramathibodi Hospital normally uses in its clinical protocols for axial head T1 and T2 weighting respectively. These series are called the site T1 and site T2 series.

For all four axial series the required slice thickness is 5 mm and the slice gap is 5mm thus, the set of eleven slice spans a distance of 100 mm from the center of the first slice to the center of the last slice.

Pulse Sequence Acquisition Parameters

Study	Pulse Sequence	TR (ms)	TE (ms)	FOV (cm)	No of Slices	Slice Thick. (mm)	Slice Gap (mm)	NEX	Matrix		Band Width (kHz)	Scan time (min:sec)
ACR Sagittal locator	Spin echo	400	10	25	1	20	20	1	256	256	2.06	0.59
ACR Axial T1	Spin echo	500	20	25	11	5	5	1	256	256	82.06	1.01
ACR Axial T2	Spin echo	2000	80	25	11	5	5	1	256	256	82.06	1.05

Table.1 ACR Pulse sequence acquisition parameters.

Table.2 Clinical protocols Pulse sequence acquisition parameters.

Study	Pulse Sequence	TR (ms)	TE (ms)	FOV (cm)	No of Slices	Slice Thick. (mm)	Slice Gap (mm)	NEX	Matrix		Band Width (kHz)	Scan time (min:sec)
ACR Axial T1	Gradient echo	150	2.3	24	11	5	5	1	256	256	173.60	1.14
ACR Axial T2	Spin echo	4000	70	24	11	5	5	1	256	256	275.15	1.15

1. Geometric Accuracy

Purpose: To assess the accuracy which the image represents lengths in the geometric test. A failure means that dimensions in the images differ from the true dimensions substantially more than $\pm 2\text{mm}$.

Method: Display the image localizer, slice 1 of the ACR T1 series, and slice 5 ACR T1 series. Seven measurements the diameters of the phantom of known lengths within the phantom are made using the display station on screen length measurement tool.

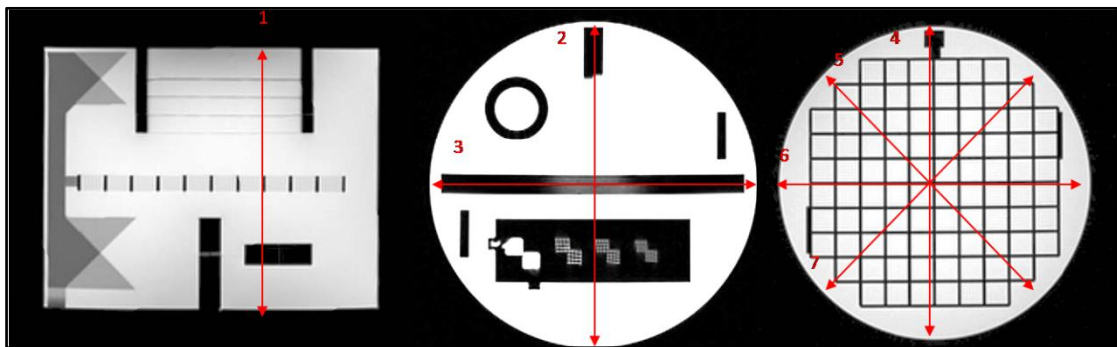


Figure. 1.0 Geometric accuracy

Table.3 Result geometric accuracy

Line No.	True Value (mm)	Sag Locator		ACR T1		ACR T2	
		Meas. (mm)	Diff (mm)	Meas. (mm)	Diff (mm)	Meas. (mm)	Diff (mm)
1	148	148.0	0.0	-	-	-	-
2	190	-	-	189	-1	189	-1
3	190	-	-	189	-1	190	0
4	190	-	-	190	0	189	-1
5	190	-	-	189	-1	188	-2
6	190	-	-	189	-1	189	-1
7	190	-	-	189	-1	189	-1

Recommended Action Criteria: $\pm 2\text{ mm}$ in all planes.

All are: Pass

2. High Contrast Spatial Resolution

Purpose: To test the scanner's ability to resolve small objects when the contrast to noise ratio is sufficiently high. A failure of this test means that for given field of view and acquisition matrix size the scanner is not resolving small details at 1.0mm .

Method: Display the slice 1 ACR axial series, magnify the image by factor of between 2 and 4, look at the rows of holes in the UL (Upper left) arrays and adjust

the display windows and level to best show the holes as distinct from one another. If all four holes in any single row are distinguishable from one another, score the image as resolved right to left at this particular hole size. Look at the hole in the LR (Lower right) array and adjust the display window and level to best show the holes as distinct from one another. Make a note of the smallest hole size resolved in each direction; that is the measured resolution for that direction.



Figure. 2 ACR protocol



Figure.3 Clinical protocols

Table.4 Result high contrast spatial resolution

	Spatial Resolution	Result
ACR Axial T1	>0.9 mm	Pass
ACR Axial T2	>0.9 mm	Pass
Clinical Axial T1	0.9 mm	Pass
Clinical Axial T2	0.9 mm	Pass

Recommended Action Criteria: 1 mm or larger

3. Image intensity Uniformity: Percent integral Uniformity (PIU)

Purpose: To measure the uniformity of the image intensity over a water region of the phantom lying near the middle of the head coil. Head coils for clinical use have fairly uniform spatial sensitivity near the middle of the coil when loaded as typical for a human head. Failure of this test means that the scanner has significantly greater variation in image intensity than 12.5 percent. Lack of image intensity uniformity

indicates a deficiency in the scanner, often a defective head coil or problem in the radio frequency subsystems.

Method: Display slice location 7. Place a large, circular region of interest on image. This ROI should have an area between 195 and 205 cm². Set the display window to its minimum, and lower the level until the entire area inside the large ROI is white. Place a small ROI roughly 1 cm² at the region of dark pixels inside the large ROI. Record the mean pixel value for this 1 cm² ROI. This is the measured low signal value. Now raise the level until all but a small, roughly 1 cm² region of white pixels remains inside the large ROI. This is the region of highest signal. Record the average pixel value for this 1 cm² ROI. This is the measured high signal value.

The measured high and low signal values for each of the ACR series are combined to produce a value called **percent integral uniformity (PIU)**. Use the following formula to calculate PIU: **PIU = 100x (1 - {(high-low)/(high+low)})**.

Table.5 Result Image intensity uniformity

	Low signal	High signal	PIU	Result
ACR Axial T1	1643.5	2248.7	84.45	Pass
ACR Axial T2	846.1	1205.7	82.47	Pass

Recommended Action Criteria: PIU should be greater than or equal to 87.5% for MRI systems with field strengths less than 3 Tesla.

4. Percent-signal ghosting

Purpose: To assess the level of ghosting in the image. Ghosts are most noticeable in the background areas of an image where there should be no signal, but usually they overlay the main portions of the image as well, artifact actually altering the image intensities. A failure of this test means that there is signal ghosting at a level significantly higher than that observed in a properly functioning scanner.

Method: Percent signal ghosting measurement is made on slice 7 of the ACR T1 series. Using the workstation's ROI tool, five intensity measurements are made: the average intensity in the primary image of the phantom, and the average intensity of the background at four locations outside of the phantom. The value for the ghosting as a fraction of the primary signal is calculated using the following formula.

$$\text{Ghosting ratio} = \frac{((\text{top} + \text{btm}) - (\text{left} + \text{right}))}{(2 \times (\text{large ROI}))}$$

Where top, btm, left, right and large ROI are the average pixel values for the ROIs of the same names. The vertical bars enclosing the right hand side of the equation mean to take the magnitude of the enclosed value.

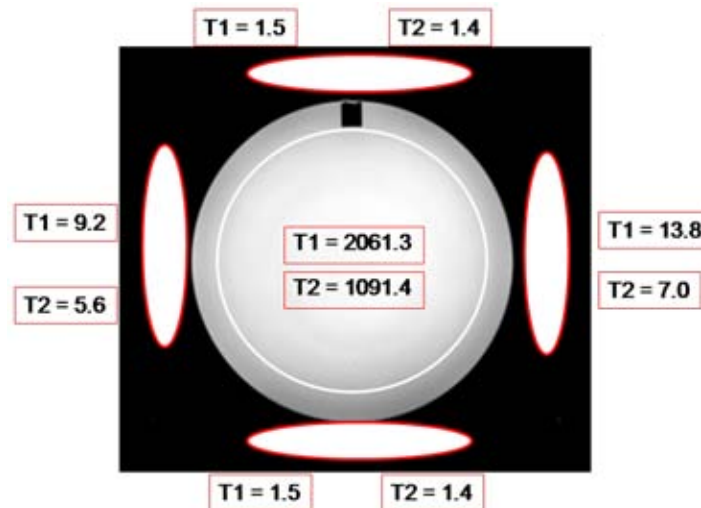


Figure.4 Percent signal ghosting

Table.6 Pixel Value

	T1	T2
Large ROI	2061.3	1091.4
Lt.ROI	59.2	5.6
Rt.ROI	13.8	7.0
TOP ROI	1.5	1.4
Bottom ROI	1.5	1.4

Table.7 Result Percent signal ghosting

	Ghosting Ratio	Result
ACR Axial T1	0.0048	Pass
ACR Axial T2	0.0044	Pass

Recommended Action Criteria: The ghosting ratio is less than or equal to 0.025.

5. Low Contrast Object Detectability

Purpose: To assess the extent to which object of low contrast are discernible in the images. The ability to detect low contrast objects is primarily determined by the contrast to noise ratio achieved in the image, and may be degraded by the presence of artifact such as ghosting. A failure of this test means the images produced by the

scanner show significantly fewer low contrast objects than most properly functioning clinical scanner.

Method: Measurements are made for the ACR and clinical series. The low contrast objects appear on four slices: slice 8 through 11. In each slice the low contrast objects appear as rows of small disks, with the rows radiating from the center of a circle like spokes in a wheel. Each spoke is made up of three disks, and there are ten spokes in each circle. All the disks on a given slice have the same level of contrast. In order from slice 8 to slice 11, the contrast value are 1.4%, 2.5%, 3.6%, and 5.1%. All the disks in a given spoke have the same diameter. Starting at the 12 o'clock position and moving clockwise, the disk diameter decreases progressively from 7.0mm at the first spoke to 1.5 mm at the tenth spoke. The measurements for this test consist of counting the number of complete spokes seen in each of the four slices. This is done for each of the four axial series.

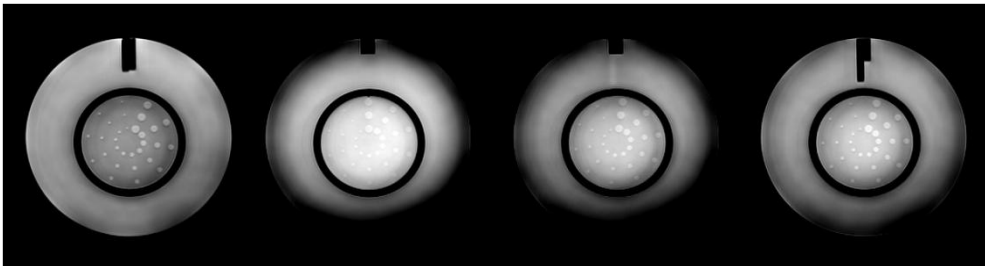


Figure.5 T1 low contrast object detectability

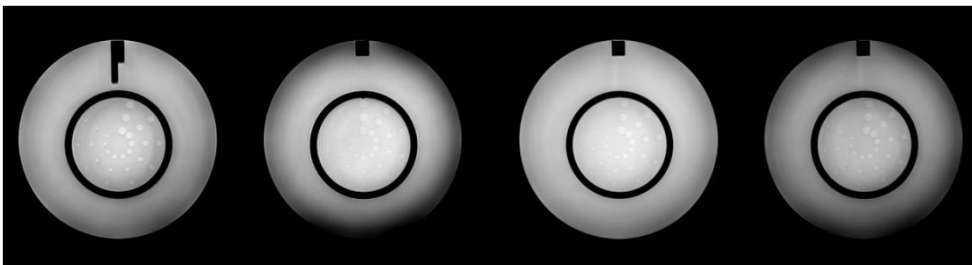


Figure.6 T2 low contrast object detectability

Table.7 Result low contrast object detectability

Contrast Value	Number of Spoke				Total	Result
	1.40%	2.50%	3.60%	5.10%		
ACR Axial T1	10	10	10	10	40	Pass
ACR Axial T2	10	10	10	10	40	Pass

Recommended Action Criteria: A total score of at least 9 spokes for MRI systems with field strengths less than 3 Tesla is accepted.

6. Slice Position accuracy

Purpose: To assess the accuracy with which slices can be prescribed at specific locations utilizing the localizer image for positional reference.

Method: Slice position accuracy test the differences between the prescribed and actual positions of slices 1 and 11 are measured. These measurements are made for the ACR T1 and T2 series. The Slice 1 and 11 are prescribed so as to be aligned with the verticals of the crossed 45° wedges at the inferior and superior ends of the phantom respectively. On slice 1 and 11 the crossed wedges appear as a pair of adjacent, dark, vertical bars at the top of the phantom. For both slice 1 and slice 11, if the slice is exactly aligned with the vertex of the crossed wedges, then the wedges will appear as dark bars of equal length on the image. By design of the wedges, if the slice is displaced superiorly with respect to the vertex, the bar on the observer's right will be longer. If the slice is displaced inferiorly with respect to the vertex, the bar on the left will be longer.

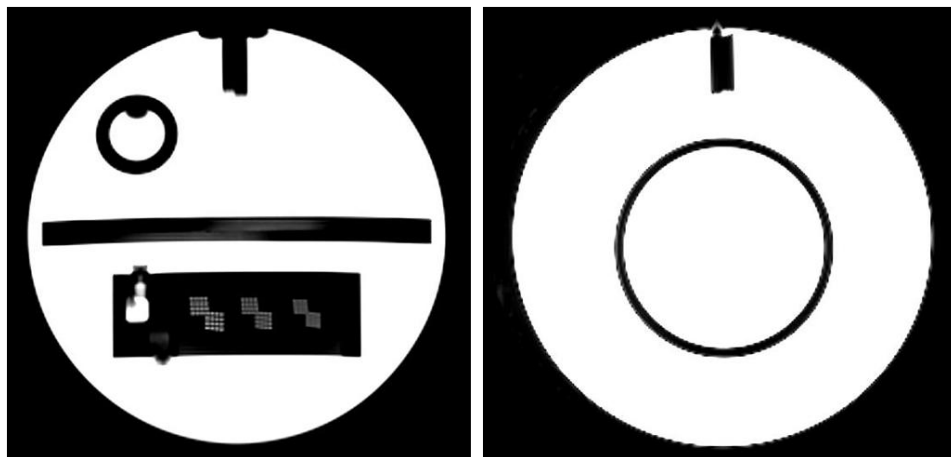
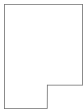
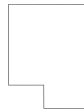


Figure.7 Slice position accuracy



Figure.8 Slice position accuracy

From slice Position 1 and 11 ACR Phantom:

Wedge (mm)	 = +	 = -	
	T1	T2	
Slice Location: 1	<u>1.6 mm</u>	<u>1.3 mm</u>	<u>Pass</u>
Slice Location: 11	<u>1.6 mm</u>	<u>1.2 mm</u>	<u>Pass</u>

Recommended Action Criteria: The magnitude of each bar length difference should be less than or equal to 5 mm.

7. Slice Thickness Accuracy

Purpose: To assess the accuracy with which a slice of specified thickness is achieved. The prescribed slice thickness is compared with the measured slice thickness. A failure of this test means that the scanner is producing slices of substantially different thickness from that being prescribed. This problem would rarely if ever occur in isolation since the scanner deficiencies that can because it will also cause other image problems. Therefore, the implications of a failure are not just that the slice are too thick or thin, but can extend to things such as incorrect image contrast and low signal to noise ratio.

Method: Slice thickness accuracy test the lengths of two signal ramp in slice 1 are measured. This is done for both ACR series. The ramps appear in a structure called the slice thickness insert. The two ramps are crossed: one has a negative slope and the other a positive slope with respect to the plane of slice 1. They are produced by cutting 1 mm wide slots in a block of plastic. The slots are open to the interior of the phantom and are filled with the same solution that fills the bulk of the phantom. The signal ramps have a slope of 10 to 1 with respect to the plane of slice 1, that is they make an angle of about 5.71° with slice 1. Therefore, the signal ramp will appear in the image of slice 1 with a length that is 10 times the thickness of the slice if the phantom is tilted in the right-left direction, one ramp will appear longer than the other. Having crossed ramps allows for correction of the error introduced by right-left tilt.

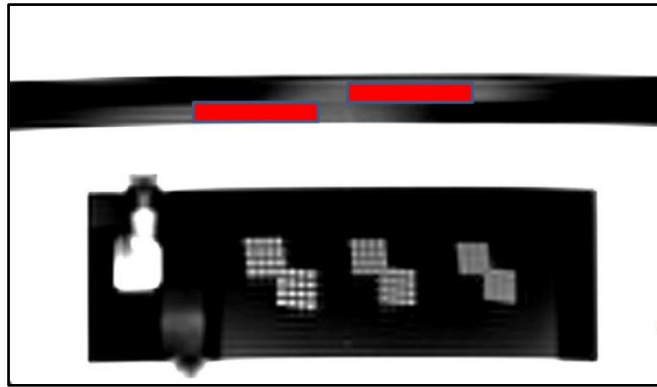


Figure.8 Magnified region of slice 1 showing slice thickness signal ramps with ROIs placed for measuring average signal in the ramps.

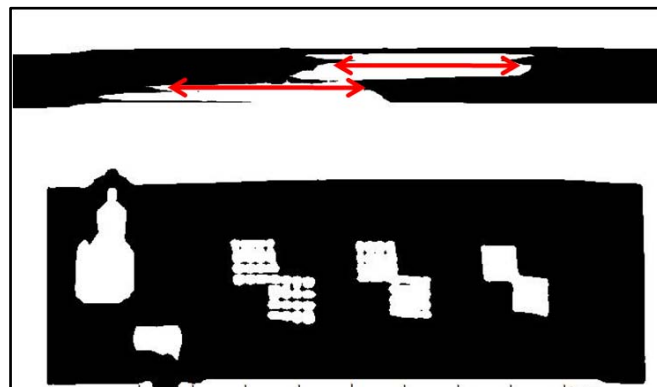


Figure.9 Magnified region of slice 1 showing slice thickness signal ramps. The display window is zero and level is half the average signal level of the ramps. The length measurement for the ramps are shown on the image

From Slice Position: 1 of the ACR Phantom:

The slice thickness is calculated using the following formula

$$\text{Slice thickness} = 0.2x (\text{top} \times \text{bottom}) / (\text{top} + \text{bottom})$$

Where top and bottom are the measured lengths of the top and bottom signal ramps.

Table.8 Result slices thickness accuracy.

Series	Slice Thickness Set (mm)	Slice Thickness Measured (mm)	Results
Brain T1	5 mm	4.8 mm	Pass
Brain T2	5 mm	4.9 mm	Pass

Slice Thickness Top: 44.9 Calculate slice
 Bottom: 53.7 (FWHM in mm) Thicknesses (mm): 4.8

Recommended Action Criteria: For both ACR series the measured slice thickness should be 5.0 mm \pm 0.7 mm.

8. Magnetic Field Homogeneity

Method Used (Spectral peak): Spectral Peak 63 Hz Phase Difference:

Measured Homogeneity: Diameter of spherical Volume (cm): 40x40x30

Homogeneity (ppm): 0.41

Vitae

Name	Mr.Adun Kampaengtip
Date of birth	September 05, 1975
Place of birth	Chiang Mai, Thailand
Education	Bachelor of Science in Radiology Technology program Faculty of Science Ramkhamhaeng University, 2001
Work Experiences	1996-Present Radiological Technologist, Advanced Diagnostic Imaging and Image-guided Minimal Invasive Therapy Center Ramathibodi Hospital, Bangkok
Award	The 2 th Best oral presentation in the title is “Technical assessment of artifact production from neuro endovascular coil at 3 Tesla MRI: an in vitro study” from 6 th Annual scientific meeting: Thai Medical Physicist Society on February 23-26, 2012, Phitsanulok, Thailand

International Congress

The 1st International Conference on Radiological Sciences and
Technology (ICRST) on October 28-30, 2011, Kobe city, Japan

The 9th South-East Asian Congress of Medical Physics
(SEACOMP), Biophysics, and Biomedical Engineering
On November 16-19, 2011, Tagbilaran City, Philippines

The 6th Annual Scientific Meeting: Thai Medical Physicist
Society on February 23-26, 2012, Phitsanulok, Thailand

Address	47/314 Mue 6 Soi Ngamwongwan 47/12 Ngamwongwan Road, Tungsonghong Laksri Bangkok 10210
----------------	--